

## Direct Plasma Measurements in the Io Torus and Inner Magnetosphere of Jupiter

FRAN BAGENAL AND JAMES D. SULLIVAN

*Center for Space Research, Massachusetts Institute of Technology, Cambridge, Massachusetts 02139*

A model of the Io plasma torus has been constructed using the in situ plasma measurements of Voyager 1. A sharp gradient in plasma temperature of  $\sim 7 \times 10^5 \text{ K } R_J^{-1}$  at  $5.7 R_J$  divides the torus into two parts, a cold inner region, where the ions are closely confined to the centrifugal equator, and a warm outer region, which includes the orbit of Io and has a thickness scale height of  $1 R_J$ . The outer edge of the warm torus is defined by a drop in plasma density near  $7.5 R_J$ . The bulk motion of the plasma, i.e., the average velocity vector, is within 1% of the value expected on the basis of strict corotation in the inner part of the torus but probably deviates by 5 to 10% from corotation outside the torus. This breakdown from corotation may occur at the outer boundary of the warm torus. The energy per charge spectra show well-resolved peaks in the inner part of the torus but strongly overlapping peaks in the outer part. In the inner torus there is a significant variation in the abundances of different ionic species over spatial scales  $< 10^4 \text{ km}$ . However, in the plasma sheet of the middle magnetosphere the ionic composition appears to be uniform from 12 to  $42 R_J$  and is strongly dominated by ions with a ratio of atomic mass to charge of 16. These ions are most probably some combination of  $\text{O}^+$  and  $\text{S}^{2+}$  ions. One consequence of the observation is that the Alfvén speed is uniformly low in the outer part of the torus, with values less than  $250 \text{ km s}^{-1}$ .

### INTRODUCTION

The dominant feature of the inner magnetosphere of Jupiter is the dense torus of plasma associated with the satellite Io. The population of heavy ions found in this region has been both a major result and a major surprise of the Voyager 1 encounter with Jupiter and is based on data of many experiments onboard the spacecraft. This paper presents the results of direct measurements of low-energy positive ions in Jupiter's inner magnetosphere within a radial distance from the planet of less than about 10 Jovian radii ( $R_J$ ) and compares the composition of the ions observed in this region with that found in the middle magnetosphere ( $R < 42 R_J$ ).

Prior to the encounter of Voyager 1 the only direct information about the properties and composition of plasma in the inner Jovian magnetosphere came from measurements carried out on Pioneer 10 and 11 by the plasma probe and ultraviolet photometer. Neither of these instruments gave results which were interpreted in terms of a dense torus of heavy ions. The Pioneer 10 plasma instrument did detect low-energy positive ions, interpreted as protons, near Io's orbit [Frank *et al.*, 1976]. Although it has subsequently been shown that these ions could not have been protons but were probably heavy ions coming from Io [Neugebauer and Eviatar, 1976; Goertz and Thompson, 1979], the experiment did not provide hard evidence concerning the plasma environment near the orbit of Io. The Pioneer 10 observations of ultraviolet radiation from the torus were interpreted as relatively weak emission from atomic hydrogen [Carlson and Judge, 1974]. The strong emission from ionized sulphur and oxygen seen by the ultraviolet spectrometer on Voyager 1 [Broadfoot *et al.*, 1979; Sandel *et al.*, 1979] was not observed by Pioneer 10, though Mekler and Eviatar [1980] have suggested that the Pioneer 10 UV observations are consistent with a torus of oxygen and sulphur ions at much lower densities than measured by Voyager.

On the other hand, ground-based optical observations of the region near Io and its orbit have revealed emission from neutral sodium [Brown, 1974] and from ionized sulphur,  $\text{S}^+$

[Kupo *et al.*, 1976]. The optical radiation observed by Kupo *et al.* came from a region inside the orbit of Io ( $5.95 R_J$ ) and was first interpreted by Brown [1976] as originating from a dense ring of cold plasma in that region. Assuming local thermodynamic equilibrium, Brown deduced limits for the electron density and temperature of  $10^{(3.5 \pm 0.5)} \text{ cm}^{-3}$  and  $10^{(4.4 \pm 0.6)} \text{ K}$ , respectively, while Mekler *et al.* [1977] concluded from the same observations  $n_e \sim 500 \text{ cm}^{-3}$  and  $T_e \sim 10 \text{ eV}$ . Although these two sets of conclusions provoked considerable discussion at the time, they certainly mark the discovery of the plasma torus at Io. The emission from  $\text{S}^+$  has been observed intermittently from the ground since the initial observations and has shown variability on time scales from less than a day [Pilcher, 1979] to more than months [Mekler and Eviatar, 1980]; variations with System III longitude are also reported [Morgan and Pilcher, 1978; Trauger *et al.*, 1980; Trafton, 1980].

On March 5, 1979, the Voyager 1 spacecraft passed (Figure 1) through both the outer (warm) and inner (cold) parts of the Io plasma torus and approached Jupiter to a periastron distance of  $4.89 R_J$ . The in situ plasma measurements showed that at the time of the encounter the outer part of the torus extended from  $\sim 7.5 R_J$  to  $5.5 R_J$ , was  $\sim 1.5 R_J$  thick, and consisted of warm ( $\sim 40 \text{ eV}$ ) sulphur and oxygen ions [Bridge *et al.*, 1979] and of predominantly cooler (of the order of  $5 \text{ eV}$ ) electrons with a smaller ( $< \sim 1\%$ ) population of hot (of the order of  $\sim 1 \text{ keV}$ ) electrons [Scudder *et al.*, this issue]. The inner part of the torus extended inward from  $5.5 R_J$  to at least the minimum distance reached by the spacecraft ( $4.89 R_J$ ). In this region the plasma was closely confined to the centrifugal equator within  $0.2 R_J$  and consisted of a cold ( $< 1 \text{ eV}$ ) multi-component plasma with positive charge density equivalent to the order of  $1000 \text{ electrons cm}^{-3}$  [Bagenal *et al.*, 1980]. Ground-based optical observations and the in situ plasma measurements of Pioneer 10 indicate significant amounts of plasma inside this distance [Pilcher, 1979; Frank *et al.*, 1976]. Voyager 1 passed under Io at 1500 UT, passing through the region where a neutral cloud of sodium normally surrounds Io. However, there was no discernible effect on the plasma that can be ascribed to the neutral cloud.

Copyright © 1981 by the American Geophysical Union.

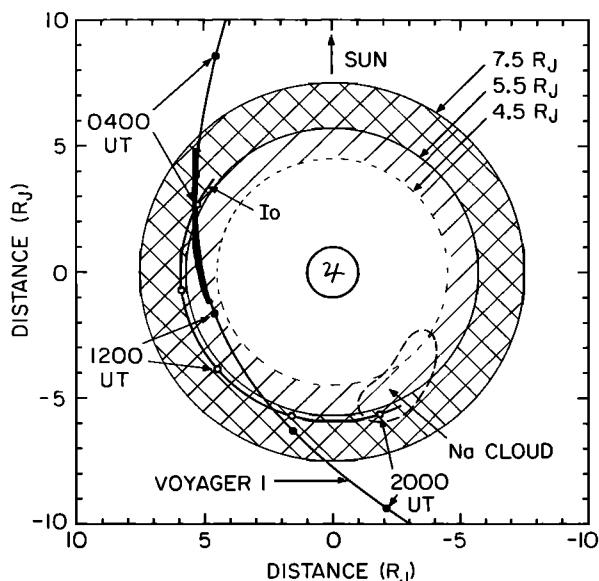


Fig. 1. Trajectory of the Voyager 1 spacecraft through the inner magnetosphere projected onto the plane of the ecliptic. Voyager 1 traversed the outer (warm) torus (crosshatched) in the midafternoon inbound and late evening outbound. The spacecraft moved through the inner (cold) torus (hatched) near closest approach. The extent of the cloud of neutral sodium atoms around Io is illustrated for 2000 UT. All the times are universal time (UT) on March 5, 1979. The orbit of Io for this period is also illustrated.

In the inner (cold) torus the plasma flow was strictly corotational with Jupiter, whereas from  $12 R_J$  outward the plasma measurements in the dayside of the magnetosphere are inconsistent with a flow that is strictly corotational [Bridge *et al.*, 1979; McNutt *et al.*, 1979; McNutt and Belcher, this issue]. The plasma data discussed in this paper are most naturally interpreted under the assumption that the warm torus plasma corotates out to about  $7.5 R_J$  but that strict corotation breaks down at this outer edge. This conclusion is in good agreement with that of Kaiser and Desch [1980], who find that the plasma at  $8-9 R_J$  rotates around Jupiter at a rate 3–5% slower than the rotation of the planet.

Initially, this paper discusses the details of positive ion measurements made in the inner magnetosphere; the analysis of those measurements to obtain plasma composition, flow speeds, and temperatures; and the assumptions made in the analysis. These results for the positive ions are then combined with the direct measurements of plasma electrons between  $5.7$  and  $9 R_J$  [Scudder *et al.*, this issue] and with a theoretical distribution of plasma along dipolar magnetic field lines to construct a two-dimensional model of the plasma torus. The implications of the model about the nature of the plasma source at Io and about subsequent transport are discussed in later sections of this paper. Finally, in a preliminary investigation of the interaction of Io with the plasma torus, the speed of propagation for Alfvén waves near Io has been calculated.

## MEASUREMENTS

### Instrument

The Voyager plasma science instrument consists of a main sensor of three modulated-grid Faraday cups (A, B, C) symmetrically positioned about an axis antiparallel to the spacecraft  $Z$  axis, which generally points away from the earth, and a fourth cup (the side sensor, D) pointed at right angles to the

$Z$  axis. A full description of the instrument is given by Bridge *et al.* [1977]. Throughout most of the inbound leg of the trajectory, before 0500 UT on March 5, 1979, the side sensor was pointed into the azimuthal flow of plasma around Jupiter. As the spacecraft approached the planet, the viewing geometry changed rapidly so that after 0500 UT the main sensor was swept into the direction of corotational flow and then rapidly away after closest approach at 1204 UT.

The response of the sensors to high sonic Mach number ( $>10$ ) plasma flow at angles  $\approx 60^\circ$  into the cups is predominantly due to geometry [Vasyliunas, 1971; see Belcher *et al.*, 1980]. For flow at more oblique angles the response is more complex, and analysis of the data on the outbound leg through the torus is as yet incomplete, although it will be eventually extended to at least  $1600$  UT ( $7 R_J$ ).

Positive ion measurements are made with each cup in the energy per charge range from 10 to 5950 V. In the high-resolution mode this voltage range is scanned in 128 steps with a resolution of  $\sim 3.6\%$ . The 128 steps are measured in 30.72 s with 96 s between adjacent scans. However, during the Jupiter encounter period, only 72 of the 128 steps were transmitted for any given 96-s measurement sequence. The two voltage ranges 10 to 750 V (steps 1 through 72) and 400 to 5950 V (steps 57 to 128) are transmitted alternately each 96 s. Hence it took 192 s to obtain a complete high-resolution spectrum. Any differences in the fluxes measured in the 16 overlapping channels indicate variations in the ambient plasma within 96 s.

Although the Voyager plasma detectors separate ions according to energy per charge, the addition of a velocity selector converts the instrument into one which selects the ions in terms of mass per charge,  $A/Z^*$ . In much of the Jovian magnetosphere the velocity selection is found by observation to be inherent; all ions corotate with the planetary magnetic field and have a common velocity perpendicular to, but not necessarily along, the field. In this circumstance, cold ions with different values of  $A/Z^*$  appear as separate peaks in the energy per charge scan of the instrument. The derivation of plasma parameters in this case is particularly straightforward.

### Derivation of Plasma Parameters

Consider a supersonic plasma in which all ions have the same average velocity but different values of atomic mass number to charge state,  $A/Z^*$ . In this case, different values of  $A/Z^*$  produce individual peaks in the energy per charge spectra and, providing that the spacecraft is uncharged, these peaks are separated by distances which are directly related to the different values of  $A/Z^*$ .

A typical well-resolved spectrum from the C sensor at  $5.3 R_J$  is shown in Figure 2. The measured currents have been converted to a 'reduced' (one-dimensional) distribution function,  $F_p$ , assuming all the particles are protons [see McNutt and Belcher, this issue]. If one assumes that all ions represented by the peaks in Figure 2 are corotating with Jupiter, i.e., they have a common flow velocity  $\vec{v} = \vec{\Omega} \times \vec{r}$ , then the values of  $A/Z^*$  are uniquely determined. Assuming corotation, the dominant peaks in Figure 2 correspond to values of  $A/Z^*$  of 8, 16, 32, and 64. A different assumption concerning the velocity would, of course, give different values of  $A/Z^*$  which are, in general, impossible or implausible on physical grounds; thus the conclusion that the plasma in the cold region of the torus moves with the velocity of corotation rests on the physical plausibility of the identifications of the spectral peaks in the spectrum of Figure 2 and in many similar spectra.

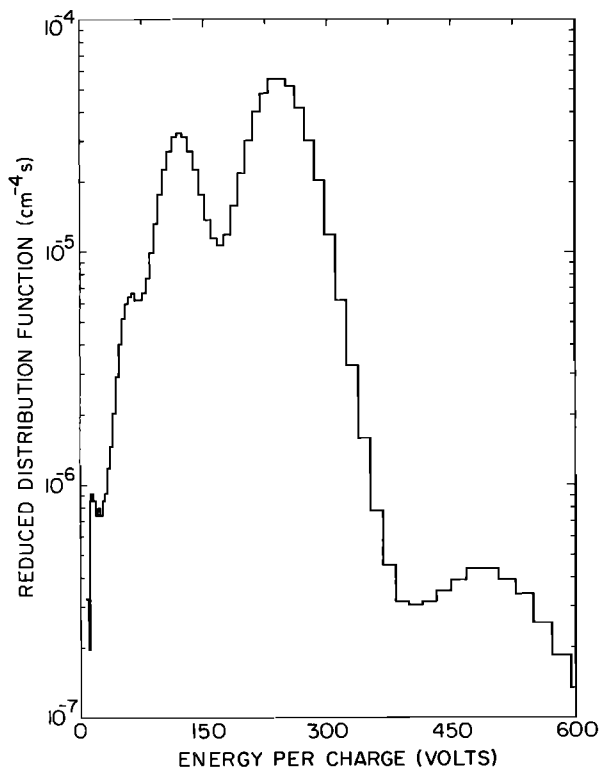


Fig. 2. An example of part of a high-resolution energy per charge spectrum from the inner (cold) torus showing peaks corresponding to ions with mass to charge ratios ( $A/Z^*$ ) of 8, 16, 32, and 64. Any protons ( $A/Z^* = 1$ ) would come below the voltage threshold of the instrument (10 V). This spectrum was made at 1016 UT.

In this discussion we have assumed that the potential of the spacecraft is zero. In fact, the spacecraft charge is not zero, and a given peak in the energy per charge spectrum is displaced by an amount proportional to the spacecraft potential multiplied by  $A/Z^*$ ; i.e., the effect is greatest for lighter ions. A comparison of the location of the well-resolved peaks in the spectra at  $A/Z^*$  values of 8, 16, and 32 indicates a spacecraft charge of  $8 \pm 5$  V in the inner torus. In the outer (warm) torus, where the spectral peaks overlap, it is not possible to measure the potential of the spacecraft directly. However, values as large as 40 V would introduce errors in relative abundances of the positive ionic species which would be smaller than the actual uncertainties in their determination due to model dependences. The possibility of the spacecraft having a potential of a much greater magnitude is discounted because of the close agreement in the values of the total charge density as determined by the plasma positive ion measurements with the values determined from observations of plasma waves by the Planetary Radio Astronomy experiment (as illustrated below).

Analysis of the resolved spectra in the cold region of the torus proceeds as follows. Each energy per charge spectrum is converted to the corresponding velocity distribution function and is analyzed using a simultaneous fit to a sum of convected isotropic Maxwellian distribution functions with the sum over the assumed values of  $A/Z^*$ . It is assumed that all species have a common bulk velocity. Spectra with well-resolved peaks (such as that shown in Figure 2) are well fit by this procedure assuming the peaks are at values of  $A/Z^* = 8, 16, 32,$  and 64. For each ionic species the fit determines the number density and thermal speed; it also determines for all species a

common component of velocity in the direction normal to each plasma sensor. For those cases where simultaneous spectra are available from the A, B, and C sensors, this procedure yields three components of the plasma velocity vector and three independent measurements of density and thermal speed.

Unfortunately, single peaks do not always correspond to a single ionic species, and the determination of kinetic temperatures is complicated for this reason. The most troublesome example in the Io torus and throughout the magnetosphere is at  $A/Z^* = 16$ , the common ratio for  $S^{2+}$  and  $O^+$ . In this example and under the assumption that the ions are isothermal, the width of the  $O^+$  peak is larger than that of the  $S^{2+}$  peak, and the experimental data can be fitted by suitable proportions of the two ions. For the spectrum in Figure 2 this procedure yields the fit shown in Figure 3. A fit which separates  $S^{2+}$  and  $O^+$  is, of course, not possible if the thermal speeds of  $S^{2+}$  and  $O^+$  are equal. However, in the region where spectral peaks are well resolved, the peaks at  $A/Z^*$  equal to 8 and 32 are presumably dominated by  $O^{2+}$  and  $S^+$  ions (although there could in principle be contributions from  $S^{4+}$  and  $O_2^+$  or  $SO_2^{2+}$ , respectively). If the peaks at 8 and 32 correspond to  $O^{2+}$  and  $S^+$  ions, then they appear to have equal temperatures. Therefore the data in the cold region of the torus have been analysed assuming that the ions are isothermal, so that  $S^{2+}$  and  $O^+$  can be separated in the cold torus.

Outside about  $5.5 R$ , the ions are warmer. Individual peaks are usually not resolved, and there is no direct evidence that the plasma is isothermal or that it moves with the corotational velocity. Thus in the warm region of the torus the results of

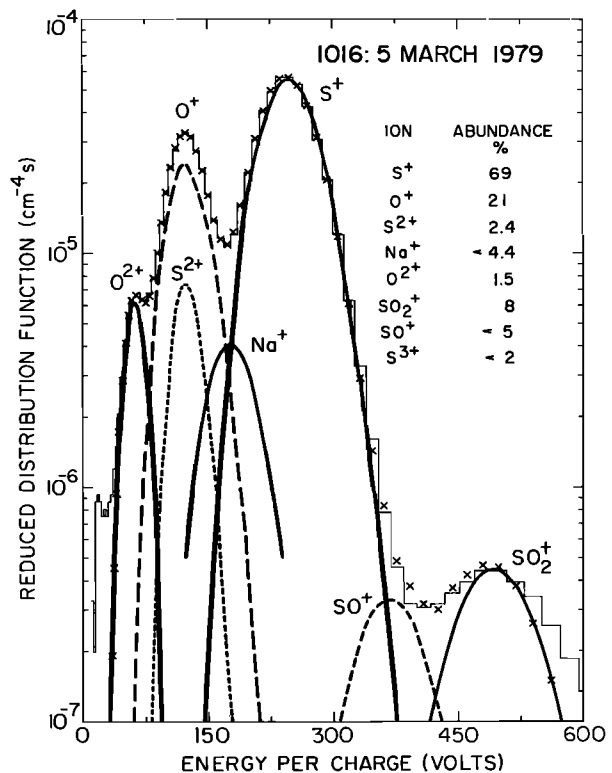


Fig. 3. The energy per charge spectrum made in the C cup of the main sensor at 1016 UT ( $5.3 R$ ), March 5, 1979. The data are shown as a histogram, and the fit to the current in each measurement channel is shown by crosses. The individual Maxwellian distributions of each ion that make up the reduced proton distribution function of the fit are shown by the curved lines.

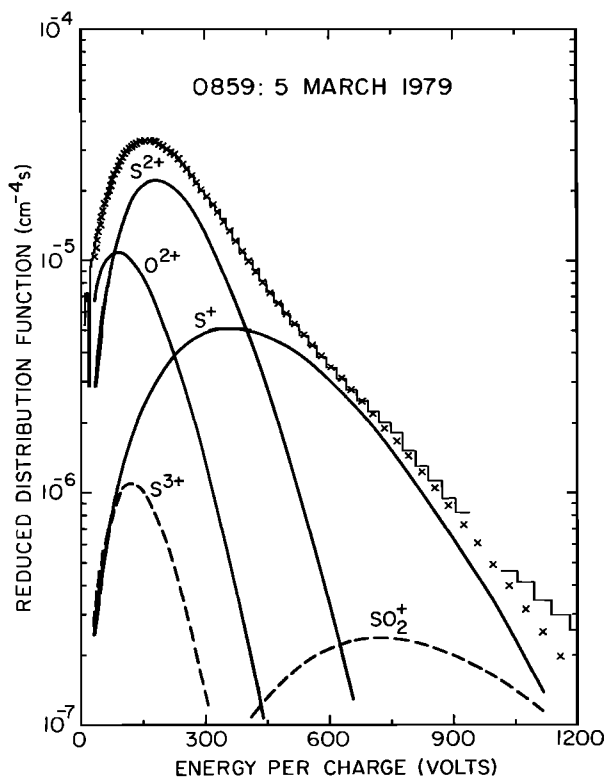


Fig. 4a. The C cup energy per charge spectrum for 0859 UT on March 5, 1979 ( $6.0 R_J$ ), which has been fitted under the assumption that all the ions are corotating with Jupiter and have the same temperature. The data are shown as a histogram, and the fit to the current in each measurement channel is shown by crosses. The individual Maxwellian distributions of each ion that make up the reduced proton distribution function of the fit are shown by the curved lines.

the fitting procedure depend critically on assumptions concerning (1) the composition, (2) the temperature, and (3) the bulk motion. The range of uncertainty in these parameters is, of course, limited by arguments of physical plausibility. Results of the fitting procedure in the warm torus and the possible range of parameters which are consistent with the data are discussed in detail in subsequent sections. An example of the fit to the data in this region is shown in Figure 4a (isothermal) and Figure 4b (common thermal speed); for both cases it was assumed that the composition was represented by the five species shown in the figure and that the bulk motion was fully corotational. The results illustrate the sensitivity of the relative abundances of  $S^{3+}$  and  $O^{2+}$  to the thermal model used in the fit.

Finally, it should be emphasized that the volume density of charge and the volume density of mass associated with a resolved spectral peak at some value of  $A/Z^*$  can be obtained directly from the analysis and that these quantities do not depend on ionic composition or charge state of the ions in the peak [Sullivan and Bagenal, 1979; McNutt and Belcher, this issue].

#### GENERAL SURVEY OF THE DATA

A comprehensive display of plasma data obtained in the torus between  $7$  and  $5 R_J$  (corresponding to the portion in the trajectory shown by the thickened line in Figure 1) is shown in the three-dimensional plot of Figure 5, where  $F_p$  is plotted against (spacecraft event) time and energy per charge. All of the 160 spectra obtained in this period are included in the

plot. After 1000 UT in the cold inner torus, three peaks stand out in the energy per charge spectra at  $A/Z^* = 32, 16,$  and  $8$ ; the relative amplitudes of these peaks vary systematically; maximum values for the individual ionic species occurred at 1030, 1050, and 1130 UT, respectively. Before 0930 UT in the outer torus the spectra are characterized by a single broad peak in  $F_p$  at about  $A/Z^* = 16$ . Noise due to interference from another instrument on the spacecraft causes the notch near 20 V in many of the 160 positive ion spectra displayed. The measured currents reached the saturation level for only one spectrum (at 0937 UT), which shows up as a spike at 300 V in this figure (the saturated channels are not plotted). The back panel shows, as a function of time, the positive charge density determined from fits to each spectrum assuming only ions with  $A/Z^*$  between 8 and 64 are present. The local maxima in the charge density profile at 0902, 0924, and 1016 UT are labeled as peaks 1, 2 and 3, respectively.

#### Charge Density

To preserve local charge neutrality, the total positive charge density must equal the electron density; thus measurements of the positive charge density should equal the total electron number density assuming that the contribution of ions with  $A/Z^* < 8$  (i.e., ions below the energy per charge threshold of the instrument) is negligible. A radial profile out to  $9 R_J$  of the electron density determined from fits to the positive ion spectra and from the Planetary Radio Astronomy (PRA) experiment [Birmingham *et al.*, this issue] is shown in Figure 6. There is close agreement between the two measurements over the entire region, indicating that most of the ions have  $A/Z^* > 8$ . Again, the three local maxima are labeled as in the previous figure.

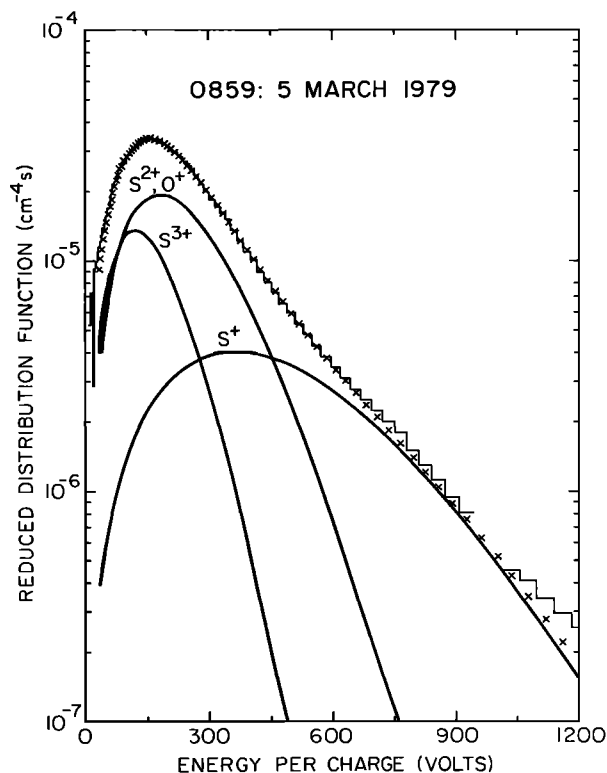


Fig. 4b. Same spectrum as Figure 4a with the fit made under the assumption that all the ions are again corotating but have a common thermal speed instead of being isothermal.

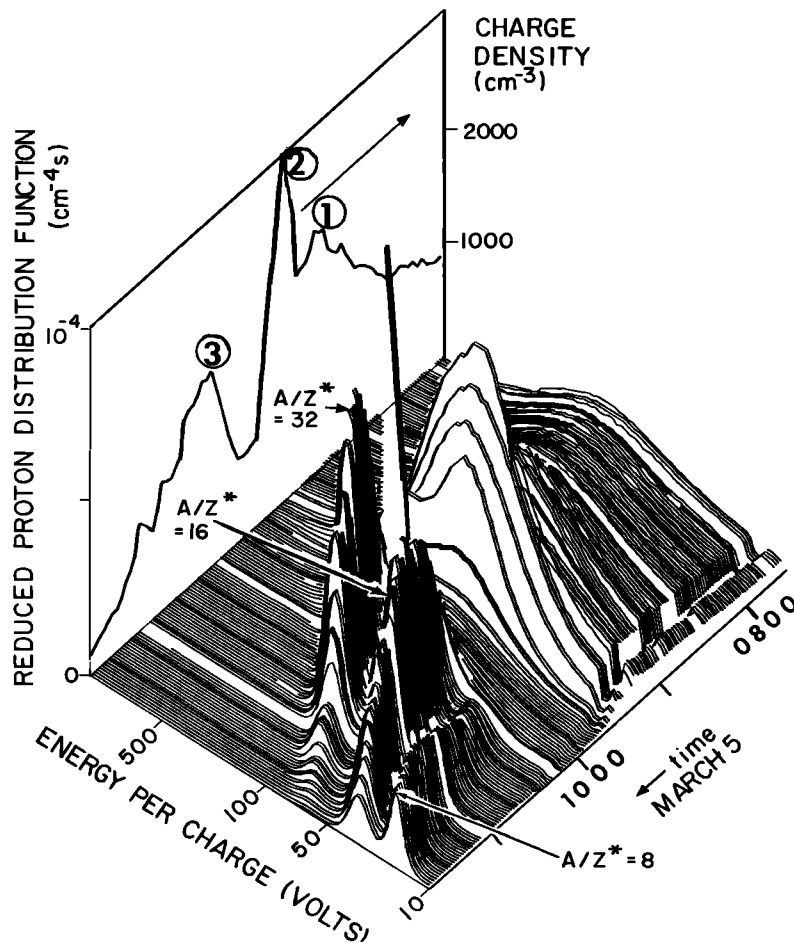


Fig. 5. A three-dimensional plot of reduced proton distribution function against energy per charge for spectral measurements made in the C cup of the main sensor between 0730 UT ( $7 R_J$ ) and 1145 UT ( $4.9 R_J$ ) on March 5, 1979. A total of 160 spectra are shown. Two spectra are omitted every 48 min, as the instrument was in a different measurement mode. Every tenth spectrum is emphasized with a darker line. The back panel shows the total positive charge density as a function of time determined from fits to the corresponding spectra.

The outer edge of the Io plasma torus is indicated by the rapid increase in density measured by both instruments as the spacecraft moved inside  $7.5 R_J$ . The density built up to a broad maximum around the orbit of Io at  $5.95 R_J$  (peak 1). The density then had a sharp peak of  $3100 \text{ cm}^{-3}$  at  $5.7 R_J$  (peak 2), well inside Io's  $L$  shell; PRA recorded a peak density of  $3500 \text{ cm}^{-3}$  around this time. However, there were few measurements of such large values, and these were all measured near  $5.75 R_J$ . The bulk of the core of the torus had a charge density from 1000 to  $2000 \text{ cm}^{-3}$ . Radially inward of  $5.7 R_J$ , the charge density dropped rapidly by a factor of  $\sim 5$  to a value of  $\sim 740 \text{ cm}^{-3}$ . As the spacecraft moved through the cold inner part of the torus, the charge density reached a second maximum of  $1740 \text{ cm}^{-3}$  at  $5.3 R_J$  (peak 3) before rapidly decreasing by an order of magnitude as the spacecraft made its closest approach to Jupiter at  $4.89 R_J$ .

Outside the torus ( $>7.5 R_J$ ) the values of charge density determined from the positive ion measurements closely match electron densities directly measured by the plasma instrument [Scudder *et al.*, this issue]. However, in the warm torus ( $5.7$  to  $7.5 R_J$ ) the spacecraft probably has a small negative charge which introduces uncertainties in the determination of the electron density from the Plasma Science experiment electron data. In the cold inner torus the energy per charge of the bulk

of the electrons was below the threshold of the plasma instrument.

#### Temperature

In the inner torus, independent determinations of the thermal speed for each ionic species from the well-resolved peaks in the spectra from all three cups of the main sensor indicate that the positively charged component of the plasma is predominantly isothermal at temperatures of a few electron volts or less. To interpret the spectra obtained in the outer part of the torus where the spectral peaks overlap, it is necessary to assume something about the thermal state of the plasma. The obvious association of the plasma torus with Io suggests that ions are produced by ionization of neutral atoms or molecules which have come from the satellite. When neutrals leave Io and are ionized, they experience a Lorentz force due to their motion relative to the corotating magnetic field; this force causes the ions to gyrate about the magnetic field at a speed equal to the magnitude of the neutral's initial velocity in the rest frame of the surrounding plasma and also causes the particles' guiding centers to move with the field. Siscoe [1977] has considered the pickup process in detail and predicted a 'tin can' velocity space distribution for each ionic species produced in this way. However, the observed torus densities are

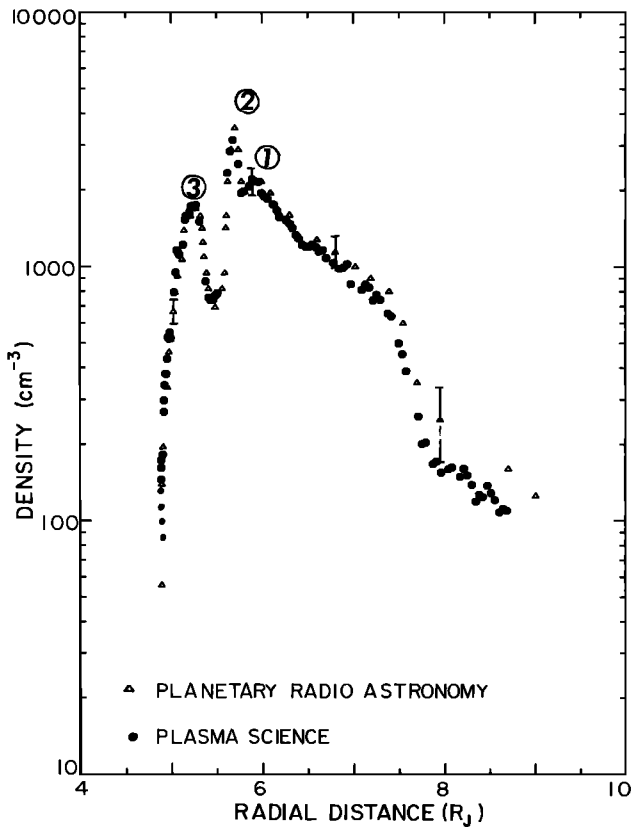


Fig. 6. Radial profile of in situ measurements of charge density. The plasma science measurements (solid circles) are of the positive charge derived from fits to positive ion energy per charge spectra. The planetary radio astronomy data (triangles) from *Birmingham et al.* [this issue] are electron density determined from the cutoff frequency of plasma wave modes (the uncertainties in the PRA determinations are shown by vertical bars).

much higher than those considered by Siscoe, so that collisions are consequently much more important. The effects of collisions over increasing time scales are first, to make the velocity distribution of each ionic species isotropic, second, to produce equipartition of energy for each species, and eventually to produce equipartition of energy between ions of different mass so that the plasma becomes isothermal. A simplistic model of an intermediate stage in this thermalization process has been made by giving the different ionic species a common 'thermal' speed.

Figure 7 shows the radial temperature profile determined from fits to the data with uncertainty limits due to model dependencies. The average ion temperature is plotted for the common thermal speed models. The outer torus had a fairly constant temperature of  $(6 \pm 1.5) \times 10^5$  K ( $\sim 50$  eV), considerably less than that expected if the gyro-speed was equal to the full corotational value. The temperature slowly increased with distance from Jupiter in the inner magnetosphere, though further out in the middle magnetosphere there are considerable variations in plasma temperature including values less than the temperatures in the outer torus [*McNutt and Belcher*, this issue]. Moving inward through the torus, the temperature decreased sharply inside  $5.7 R_J$ , dropping by a factor of 50 to less than 1 eV. This sharp transition is the division between the inner (cold) torus and the outer (warm) torus and occurs in the same region that the plasma density decreased by a factor of 5.

Throughout the torus, significant particle fluxes were detected at energies well above the energy of the bulk of the plasma. For example, Figure 8 shows the spectrum at  $5.4 R_J$  (1000 UT). This spectrum was previously presented by *Sullivan and Bagenal* [1979] to illustrate the initial interpretation of these high-energy fluxes as small quantities of molecular ions with  $A/Z^*$  ratios of  $\sim 104$  and  $\sim 160$ . This interpretation was made under the assumptions that all the plasma had a common bulk velocity and a single thermal state. An alternative interpretation is possible if the plasma is not characterized by a single thermal state. There is a sharp cutoff in the energy per charge spectrum above which the fluxes become negligible. This cutoff in the spectrum may be indicative of ions which have been recently ionized and hence have a non-Maxwellian distribution. This cutoff at 1400 V corresponds to the energy per charge of freshly ionized  $S^+$  ions with a gyro-speed of  $59 \text{ km s}^{-1}$  and a component of corotation into the sensor of  $33 \text{ km s}^{-1}$ . Lighter ions such as oxygen would have lower cutoffs and may correspond to features in the spectra such as the shoulder previously interpreted as being due to ions with  $A/Z^* = 104$ . From 0937 UT ( $5.8 R_J$ ) onward until periapsis, all the spectra have a similar cutoff. Outside  $5.8 R_J$  (before 0937 UT) the spectra do not have a high-energy cutoff below 6 KeV. This absence of a cutoff suggests that in the outer region of the torus the plasma has gained energy via a mechanism other than recent ionization. Alternatively, it is possible that the high-energy tail might be due to very heavy ions with  $A/Z^* > 300$ .

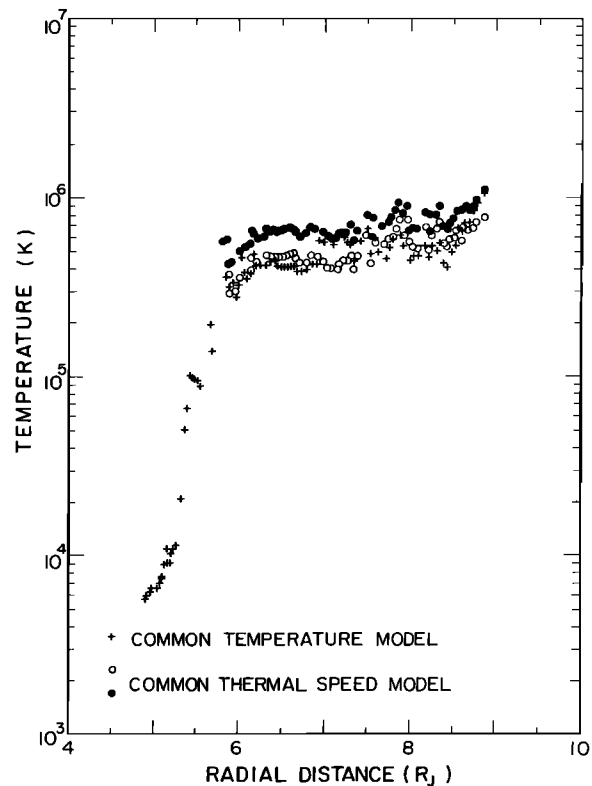


Fig. 7. Radial profile of ion temperature derived from fits to the positive ion energy per charge spectra. The crosses are from the fits where the ions are assumed to have the same temperature. With the common thermal speed model the average ion temperature has been calculated assuming the  $A/Z^* = 16$  spectral peak to be all  $S^{2+}$  (solid circles) or all  $O^+$  (open circles).

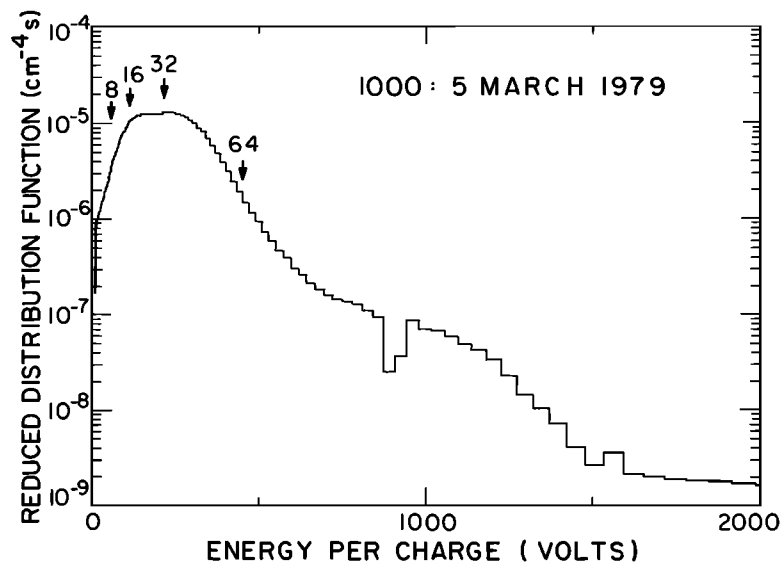


Fig. 8. C sensor energy per charge spectrum obtained on day 64 at 1000 UT ( $5.4 R_J$ ). The arrows mark the locations of various  $A/Z^*$  values assuming strict corotation. The notch at  $\sim 30$  V is caused by interference from another experiment on the spacecraft.

### Bulk Motion

In fitting the positive ion spectra, it is necessary to assume either a bulk flow or a particular composition. In the cold inner torus, assigning the three main peaks  $A/Z^*$  ratios of 8, 16, and 32 suggests that the ions had the same average component of velocity into each sensor and that value was within 1% of the value expected for corotation (compare Figure 3). Since all three cups of the main sensor collected large fluxes at this time, the components of the bulk velocity of the plasma into each cup can be combined to construct the velocity vector of the plasma flow. When these in situ flow velocity measurements were combined with the local magnetic field measured by the Voyager magnetometer (N. F. Ness, private communication, 1979), the plasma had a small field-aligned component in the same direction as the magnetic field. Measurements of the plasma flow velocity vectors will be discussed in a future publication.

Outside the torus at radial distances greater than  $12 R_J$ , there are several well-resolved peaks in the energy per charge spectra which could not be associated with any reasonable combination of  $A/Z^*$  values if the plasma is taken to be corotating [Sullivan and Bagenal, 1979; McNutt et al., 1979; McNutt and Belcher, this issue]. Figure 9 shows the last high-resolution spectrum with well-resolved peaks which was observed at  $11.8 R_J$ , well before the spacecraft entered the torus. A consistent assignment of  $A/Z^*$  ratios of 1, 8,  $10^2/3$ , 16, 23, and 32 indicates the plasma is moving at about 80% of the corotational speed. Therefore the assumption of full corotation of the plasma must break down somewhere between  $5.4$  and  $12 R_J$ .

Between  $5.5$  and  $9 R_J$ , the energy per charge spectra of the positive ions (Figure 5) are generally dominated by a single broad peak in  $F_p$ , and there is an additional uncertainty in any fitting procedure. In the fits to data taken in this region (compare Figure 4) the plasma has been assumed to be corotating, and the bulk speed was not a parameter of the fit. Allowing the bulk speed to be a free parameter of the fit in the warm torus produces values which are consistent with corotation, though deviations of up to 10% are not ruled out. Just outside

the torus, if the component of bulk flow into the cup is made a free parameter in the fit, the resulting value is usually found up to 10% below the corotation value, though the fits are by no means unique. Figure 10 shows the fit to a spectrum at

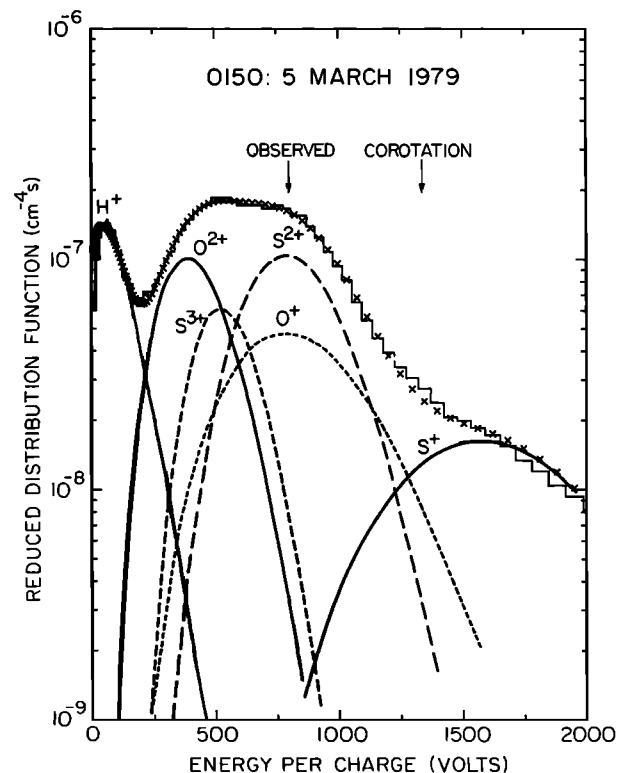


Fig. 9. The energy per charge spectrum in the D cup (side sensor) at 0150 UT, March 5, 1979 ( $11.6 R_J$ ). The position of the spectral peak due to ions with  $A/Z^* = 16$  and a bulk velocity corresponding to corotation is shown (by the arrows) to be at a considerably higher energy per charge than that determined from the fit to the observed spectrum. The data are shown as a histogram, and the fit to the current in each measurement channel is shown by crosses. The individual Maxwellian distributions of each ion that make up the reduced proton distribution function of the fit are shown by the curved lines.

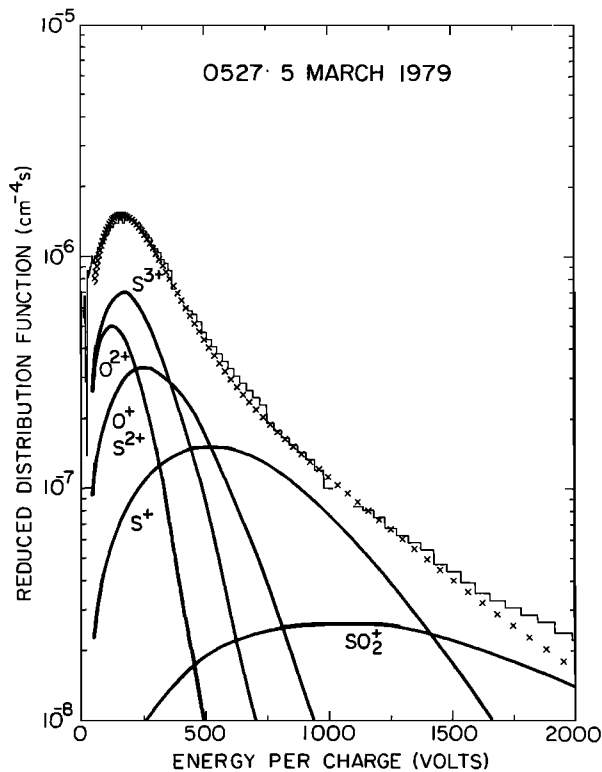


Fig. 10a. The energy per charge spectrum in the C cup at 0527 UT, March 5, 1979 ( $8.6 R_J$ ), which has been fitted assuming all the ions have the same thermal speed and have a bulk velocity corresponding to corotation with Jupiter. The data are shown as a histogram, and the fit to the current in each measurement channel is shown by crosses. The individual Maxwellian distributions of each ion that make up the reduced proton distribution function of the fit are shown by the curved lines.

0527 hours ( $8.4 R_J$ ) assuming the plasma flow is fully corotational (Figure 10a) and 90% of the corotational value (Figure 10b). The corotational fit produces a larger proportion of  $O^{2+}$  ions than that found under the same assumptions closer to Jupiter (e.g., at 0859 in Figure 4). Allowing a 10% deviation of the flow from full corotation produces a composition more similar to that at 0859. Following a similar procedure at 0720 ( $7 R_J$ ), the fit with 90% corotational flow produced relatively large proportions of  $SO_2^+$  ions. It seems quite reasonable that corotation should break down between 7 and  $8 R_J$ , as this region coincides with the outer edge of the torus at  $7.5 R_J$ . Additional evidence of the deviation of the plasma flow from corotation at  $8-9 R_J$  is found in the plasma wave observations of Kaiser and Desch [1980].

The plasma parameters discussed in this paper have been derived assuming full corotational flow between  $5.4$  and  $7.5 R_J$ , allowing  $<10\%$  deviation from corotation between  $7.5$  and  $9 R_J$  and using the spectral peaks to determine flow speed in the remaining regions.

#### Composition

Throughout the inner magnetosphere there is considerable variation in the relative abundances of the different ionic species that compose the positively charged component of the plasma. The spectra in Figure 5 illustrate the varied nature of the plasma in the inner magnetosphere. For example, in the inner part of the torus a comparison of the spectrum in Figure 11 taken at  $4.96 R_J$ , with the spectrum in Figure 3 taken at  $5.3$

$R_J$  shows the considerable variation in composition in the region. The variability in relative abundance is less marked in the outer torus and further out in the plasma sheet of the middle magnetosphere.

The existence of resolved spectra at both larger and smaller radial distances suggests that the broad spectral feature observed between  $5.7$  and  $12 R_J$  consists of the sum of peaks corresponding to a similar set of ionic species. Ions at higher temperatures have wider distribution functions and hence may combine together to form a single broad spectral peak. There is additional evidence for the presence of several ionic species from the shoulder at higher energy per charge due to ions of  $A/Z^* = 64$  and from variations in the shape of the broad peak when the plasma cools sufficiently to make two peaks discernible. If the single peak in the outer torus did in fact correspond to just one corotating ionic species, then it would have an  $A/Z^*$  ratio of  $\sim 14$  and a temperature of  $\sim 150$  eV. However, the distributions are poorly represented by a single Maxwellian function. The evidence for several different ionic species at these radial distances is consistent with observations of substantial intensities of ultraviolet radiation emitted by  $S^{3+}$ ,  $S^{2+}$ , and  $O^{2+}$  [Broadfoot *et al.*, 1979] as well as the ground-based optical observations of  $S^+$  and  $O^+$  [Pilcher, 1979; Pilcher and Morgan, 1979].

Table 1 presents in situ densities of various ionic species determined from fits to energy per charge spectra at  $4.96$  and  $5.3 R_J$  (in the inner (cold) torus),  $6.0 R_J$  (in the warm (outer) torus), just outside the torus ( $8.6 R_J$ ), and at four of many locations in the middle magnetosphere plasma sheet where there are well-resolved spectral peaks ( $11.8$ ,  $20$ ,  $28$ , and  $42 R_J$ ). Each of these eight positive ion spectra is representative of the plasma in these respective regions. At  $6.0$  and  $8.6 R_J$ , the re-

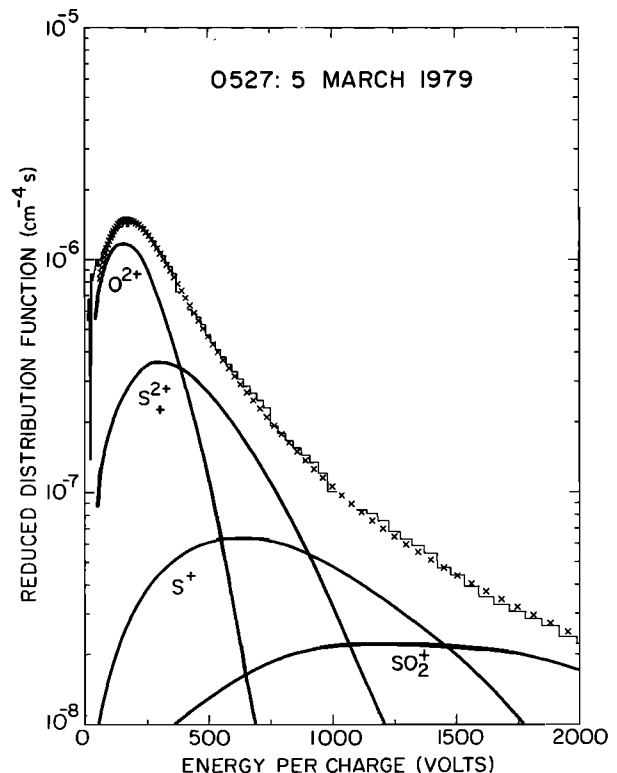


Fig. 10b. Same spectrum as Figure 10a fitted assuming the ion bulk velocity to be in the direction of corotation but only 90% of the corotational value.

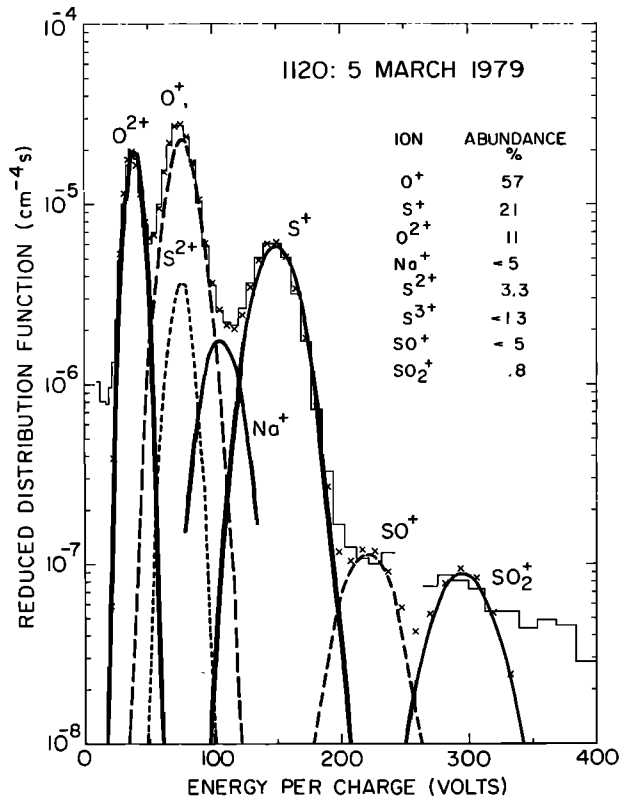


Fig. 11. The energy per charge spectrum made in the C cup at 1120 UT, March 5, 1979 ( $\sim 5 R_J$ ). The data are shown as a histogram, and the fit to the current in each measurement channel is shown by crosses. The individual Maxwellian distributions of each ion that make up the reduced proton distribution function of the fit are shown by the curved lines.

sults of fitting the spectra under each thermal model are tabulated. For example, the spectrum at 0859 in Figures 4a and 4b shows that both thermal models pick out the main peak at  $A/Z^* = 16$  as the dominant contributor. When all the ions are assumed to have a common thermal speed, the low-energy shoulder to the peak is best fitted with  $S^{3+}$  at  $A/Z^* = 10^{2/3}$  rather than  $O^{2+}$  at  $A/Z^* = 8$  as in the case of the common temperature assumption. The shoulder at higher energy per charge is largely at  $A/Z^* = 32$  ( $S^+$  or  $O_2^+$ ) in both cases. If the  $A/Z^* = 16$  peak in the common thermal speed fit is all  $S^{2+}$ , then the composition is almost entirely sulphur ions at a temperature of  $\sim 40$  eV. Alternatively, if the peak at  $A/Z^* = 16$  is all  $O^+$ , the plasma would have a lower average temperature ( $\sim 20$  eV). The common temperature fit produces a temperature of 28 eV and includes both  $S^{2+}$  and  $O^+$ .

The discussion above has been confined to the ionic species that dominate the plasma in number density. There is also evidence for various minor species. Sometimes there is a resolved spectral peak such as the proton peak in Figure 8, the  $SO_2^+$  peak in Figure 3, or the  $Na^+$  peak in Figure 1 of Sullivan and Bagenal [1979]. At other times the minor species may produce a shoulder on the edge of a spectral peak (for example,  $SO_2^+$ ). Finally, upper limits can be put on the densities of ions which come between two resolved spectral peaks as illustrated for  $Na^+$  and  $SO^+$  in Figure 3. When fitting a gap in a spectrum between two peaks, the minor ionic species is chosen for its plausibility. An upper limit for the density of any other ionic species with a similar  $A/Z^*$  ratio could be determined in the same way.

In the middle magnetosphere, protons compose up to  $\sim 30\%$  of the number density, their importance increasing with distance away from the plasma sheets [McNutt and Belcher, this issue]. In the inner magnetosphere the kinetic energy of pro-

TABLE 1. Composition of the Plasma in the Dayside Magnetosphere of Jupiter

| $A/Z^*$ | Ion      | March 5                |                       |                       |                       |                        | March 4              |                      |       | March 3,<br>1031 UT,<br>42 $R_J$ |
|---------|----------|------------------------|-----------------------|-----------------------|-----------------------|------------------------|----------------------|----------------------|-------|----------------------------------|
|         |          | 1120 UT,<br>4.96 $R_J$ | 1016 UT,<br>5.3 $R_J$ | 0859 UT,<br>6.0 $R_J$ | 0527 UT,<br>8.6 $R_J$ | 0150 UT,<br>11.7 $R_J$ | 1550 UT,<br>20 $R_J$ | 0505 UT,<br>28 $R_J$ |       |                                  |
| 1       | $H^+$    |                        |                       |                       |                       | 2.2                    | 0.21                 | 0.06L                | 0.06L |                                  |
| 8       | $O^{2+}$ | 48                     | 26                    | 160                   | 28                    | 20                     | 1.5                  | 0.10*                | 0.03* |                                  |
| 10      | $S^{3+}$ | <5.6                   | <3.5                  | 27                    | ...                   | 0.5                    | 0.6                  | 0.09*                | 0.05* |                                  |
| 16      | $S^{2+}$ | 14                     | 39                    | 170*                  | ...                   | 11*                    | 2.2                  | 0.39†                | 0.17† |                                  |
| 16      | $O^+$    | 350                    | 250                   | 560                   | 16†                   | 12†                    | 2.9                  | 0.78‡                | 0.35‡ |                                  |
| 23      | $Na^+$   | <21                    | <72                   | 1100†                 | 32†                   | 24†                    |                      | 0.08*                | 0.05* |                                  |
| 32      | $S^+$    | 91                     | 1100                  | 430                   | 8                     | 28                     | 1.4                  | 0.09*                | 0.07* |                                  |
| 48      | $SO^+$   | <2                     | <8                    | 470*                  | 11*                   | 23*                    |                      |                      |       |                                  |
| 64      | $SO_2^+$ | 3.5                    | 13                    | 73                    | 7                     | 7                      |                      |                      |       |                                  |
|         |          |                        | 8*                    | 8*                    | 8*                    |                        |                      |                      |       |                                  |
| $V_c$   |          | 62                     | 66                    | 75                    | 108                   | 148                    | 251                  | 351                  | 527   |                                  |
| $V/V_c$ |          | 1.0                    | 1.0                   | 1.0                   | 1.0                   | 0.9                    | 0.77                 | 0.76                 | 0.49  |                                  |

L, determined from low-resolution spectra [McNutt and Belcher, this issue]. All densities (in  $cm^{-3}$ ) are derived from the isothermal model for the ions unless otherwise noted.  $V_c$  is in kilometers per second.

\*From constant thermal speed model.

†From constant thermal speed model when  $A/Z^* = 16$  spectral peak is assumed to be all  $S^{2+}$ .

‡From constant thermal speed model when  $A/Z^* = 16$  spectral peak is assumed to be all  $O^+$ .

tons is generally insufficient to produce measurable fluxes above the energy per charge threshold of the plasma instrument. However, there are a few spectra before closest approach (where the cold plasma flows directly into one of the cups) with a feature which might be the tail of a distribution function in the lowest channels, below the well-resolved  $A/Z^* = 8$  spectral peak. If this feature corresponds to either  $H^+$  or  $He^{2+}$  ions with the same temperature as the heavy ions, then a fit to the data gives density estimates of  $\sim 16$ , or  $1.8 \text{ cm}^{-3}$ . This is about 3%, or 0.4% of the total ion number density. These values should be regarded with extreme caution because the density is estimated from the tail of the distribution, since the data do not include the peak.

The well-resolved spectral peaks found in cold regions of the middle magnetosphere suggest sodium ions form about 10% of the ionic composition with densities a little less than those of ions with  $A/Z^* = 32$ . In the inner torus, filling the gap between the peaks at  $A/Z^* = 16$  and 32 with the appropriate amount of  $A/Z^* = 23$  suggests that sodium is relatively less abundant closer in, forming less than  $\sim 5\%$  of the ion composition. From the densities in the middle magnetosphere and a simplified model of steady state flux tube interchange diffusion [Siscoe, 1978], a sodium ion source strength of the order of  $10^{25} \text{ ions s}^{-1}$  has been derived. This value is consistent with the calculations of Smyth and McElroy [1978] based on optical measurements of the neutral sodium gas cloud around Io. It should be noted that these relative abundances for sodium are measurements made along the spacecraft trajectory and that the variation in their value may be due to effects of magnetic latitude as well as radial distance.

There is often a well-defined spectral peak corresponding to  $A/Z^* = 64$  (Figure 3) which is probably  $SO_2^+$  (or maybe  $S_2^+$ , which has the same  $A/Z^*$  ratio). Fitting the  $A/Z^* = 64$  peak at  $5.3 R_J$  produces a density of  $\sim 13 \text{ cm}^{-3}$ , which is  $< 1\%$  of the ion population. When the plasma becomes too hot for separate spectral peaks, then the density of the ion with  $A/Z^* = 64$  (taken to be  $SO_2^+$ ) can be found from a well-defined shoulder. The  $SO_2^+$  density in the warm torus has a maximum value around Io's orbit of  $\sim 8 \text{ cm}^{-3}$  ( $< 1\%$  of the ions) for the common thermal speed model and  $\sim 73 \text{ cm}^{-3}$  ( $\sim 5.5\%$  of the ions) for the isothermal model. The relative abundance of  $SO_2^+$  increased outside the torus to  $\sim 10\%$  at  $8.6 R_J$ , before the  $A/Z^* = 64$  peak disappeared above the energy range of the instrument. Filling the gap between the  $S^+$  and  $SO_2^+$  peaks in the 1016 UT spectrum (Figure 3) produces an upper limit of  $8 \text{ cm}^{-3}$  ( $\sim 0.5\%$  of the ions) for  $SO^+$ .

Finally, it should be noted that the upper limits on the densities of minor species discussed above are speculative and some of these spectral features could well be due to alternative minor ionic species to those suggested or due to non-Maxwellian components in the distribution of the major ions.

#### SPATIAL VARIATION OF PLASMA PROPERTIES

##### *Model of the Torus*

A two-dimensional model of the torus can be constructed from the in situ density measurements made along the spacecraft trajectory by assuming the distribution of plasma along the magnetic field lines. Warwick *et al.* [1979] took the electron densities determined from radio data (PRA experiment) obtained on both inbound and outbound legs of the trajectory and drew contours of constant density in a meridional plane by assuming the torus to be symmetric both azimuthally and about the magnetic equator. Bagenal *et al.* [1980] inserted the

ion temperature determinations from inbound measurements into a simple expression for an exponential scale height distribution and extrapolated the in situ ion density measurements along dipolar magnetic field lines. Azimuthal symmetry was again used with mirror symmetry about the centrifugal equator to construct meridional contour maps of ion and electron densities. In this paper the azimuthal symmetry assumption is removed, the maximum radial distance has been increased from 7 to  $9 R_J$ , and measurements of the temperature of the electron population [Scudder *et al.*, this issue] have been included outside  $5.7 R_J$ . The resulting two-dimensional model of the torus reflects a more realistic geometry for the magnetic field and includes the significant interaction between the different ionic species as well as their interaction with the electrons.

The details of the method used to extrapolate the plasma measurements are discussed in the appendix. The exponential scale height distribution of Hill and Michel [1976], previously applied to some of the plasma data [Bagenal *et al.*, 1980], has been replaced by expressions which include the electrostatic interaction between different ionic species. However, the concept of a 'scale height' is a useful one, so it has been used to give an approximate idea of how rapidly the density varies with distance from the centrifugal equator.

A centered tilted dipole magnetic field has been used to determine the geometry of a field line in the meridional plane at the instantaneous longitude (System III) of the spacecraft at the time of each measurement on the inbound leg of the trajectory. Then the plasma density and temperature along the instantaneous field line is computed using the expressions derived in the appendix to extrapolate the local charge density. Finally, by linearly interpolating between the calculated densities, the plasma densities have been mapped out on a surface that makes a cross section of the torus. The surface includes the inbound spacecraft trajectory and the dipole magnetic field line associated with the location of the spacecraft at the time of each measurement. The resulting contour map of total charge density on this surface is shown in Figure 12 as a plot of density as a function of radial distance from the center of Jupiter and distance from the centrifugal symmetry surface (centrifugal equator). The apparent asymmetry about the centrifugal equator is due to the geometry of the tilted dipole. While both the inbound and outbound trajectories of the spacecraft are shown, the map is based solely on data obtained on the inbound pass.

Outside the torus ( $> 7.5 R_J$ ) the plasma had a fairly uniform low density of  $\sim 100 \text{ cm}^{-3}$ . As Voyager 1 moved radially inward, the density rapidly increased as the spacecraft entered the torus (at  $\sim 7.5 R_J$ ) from below the centrifugal equator. After crossing the equator at  $\sim 7.1 R_J$ , the spacecraft remained less than  $0.15 R_J$  above and traversed the core of the warm torus, passing over the small region of the peak torus density ( $\sim 3000 \text{ cm}^{-3}$ ) at  $5.8 R_J$ , which corresponds to the sharp spike (peak 2) in the in situ density profile (Figure 6). The plasma in the outer part of the torus was warmer and hence spread away from the equatorial maximum with an effective exponential scale height of  $\sim 1 R_J$ . Inside the sharp temperature drop at  $5.7 R_J$ , the plasma was cold and hence closely confined to the centrifugal equator with an effective scale height of  $< 0.2 R_J$ . The centrifugal equator was crossed again in the locality of the peak density in the inner torus at  $\sim 5.3 R_J$  (peak 3).

The two-part nature of the plasma torus is apparent in Figure 12 and in the radial profiles of charge density (Figure 6)

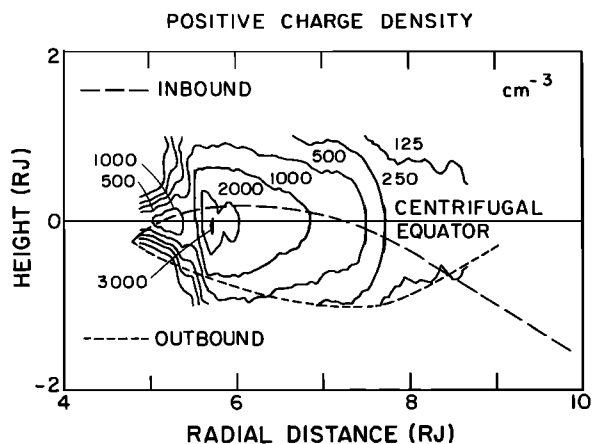


Fig. 12. Contour map of positive charge density as a function of radial distance from the center of Jupiter and height from the centrifugal equator. The map has been constructed from plasma measurements made along the inbound spacecraft trajectory (dashed lines) by using a theoretical expression for the distribution of plasma along dipolar field lines.

and ion temperature (Figure 7). Between the two parts of the torus the spacecraft passed through a transition region, where there was a sharp temperature gradient of  $\sim 7 \times 10^5 \text{ K } R_j^{-1}$ . The transition region around  $5.5 R_j$  is also one of the three regions where whistler mode plasma waves were observed by the Voyager 1 plasma wave science (PWS) experiment [Gurnett *et al.*, 1979]. The other two regions were at  $\sim 6 R_j$  on both inbound and outbound legs of the trajectory. The measured frequency dispersion of the whistlers is largely determined by the density of electrons in the plasma through which these waves have propagated. Gurnett *et al.* [this issue] conclude that the dispersion of these whistlers suggests there are considerably more electrons between the point of measurement and the source of the whistlers in the ionosphere of Jupiter than are accounted for in this model of the torus. If there are additional electrons, they could be associated with light ions such as protons which would not be as closely confined to the centrifugal equator as the heavy ions. These light ions would have larger effective scale heights so that they would form a small proportion of the plasma near the equator (where the measured total positive charge density is very close to the electron density) but could dominate the ion composition closer to the planet. Determining the density of ions outside the torus region might give an estimate of the importance of the ionosphere of Jupiter as a source of plasma for the magnetosphere.

#### Radial Structure

Although the plasma detector was less favorably oriented on the outbound traversal of the torus, considerable fluxes were measured. The global structure on the outbound pass was found to be very similar to the inbound (for a three-dimensional plot of the outbound data analogous to Figure 5, see Belcher *et al.* [this issue]). Although a similar global structure was indicated by both inbound and outbound passes through the torus, the lower density measured during the outbound passage is due to the greater distance of the spacecraft from the centrifugal equator. This effect is especially noticeable in the inner torus, where the effective scale height is small.

The magnitude and location of the three local density maxima (peaks 1, 2, 3) and the location of the transition region

and the outer boundary are shown in Table 2. The local density maxima on the outbound trajectory have been found from the PRA and plasma profiles; peak 3 outbound does not correspond to the close approach to the Io flux tube [Belcher *et al.*, this issue]. Although the radial distances of the first and second peaks vary by  $0.2 R_j$  between the inbound and outbound passes, the  $L$  shells of the maxima nearly coincide when the offset of the magnetic dipole from the center of Jupiter is taken into account. If the offset of the field were neglected, then the electron densities determined by Birmingham *et al.* [this issue] would be larger than the values along the outbound trajectory shown in Figure 12 by about a factor of 2 at  $\sim 6 R_j$ , and to a lesser extent further out. The effect of including the dipole offset is to change the apparent outbound trajectory shown in Figure 12 with the result that the electron densities (Table 2) predicted from the inbound plasma data are in good agreement with those determined by Birmingham *et al.* [this issue].

#### Azimuthal Structure

In the two-dimensional model of the torus of Figure 12 there is no information about azimuthal structure because each measurement was made at a different System III longitude. With a more sophisticated analysis of the outbound plasma data, it will be possible to compare plasma parameters at the same  $L$  shell but at two System III longitudes as much as  $\sim 170^\circ$  apart and at two local times as much as 9 hours apart.

Significant variations of plasma properties with System III longitude of Jupiter are evident from ground-based optical observations [Morgan and Pilcher, 1978; Trauger *et al.*, 1980; Trafton, 1980]. The optical emission is mainly from  $S^+$  ions in the cold region of the torus which were sampled by Voyager 1 in a small range of System III longitudes. From many observations made between 1976 and 1979, Trafton [1980] showed the emission to be enhanced as much as a factor of 5 at longitudes around  $\sim 260^\circ$ . Morgan and Pilcher [1978] saw increased emission at similar longitudes in early 1978. However, Trauger *et al.* [1980] report that on a single night in 1976 there was a comparable depletion in the emission at  $\sim 280^\circ$  System III longitude which may reflect fluctuations in the plasma torus due to spurts of volcanic activity on Io.

Longitudinal variations in the ultraviolet emissions from the outer (warm) torus are not evident from the Voyager data, though the experimenters report that the emission intensities from the dusk quadrant (local time) are enhanced by a factor of  $\sim 2$  [Sandel, 1980]. As these variations in emission with System III longitude and local time are not reflected in the plasma ion measurements, they may be caused by changes in the thermal properties of the electrons.

#### Small-Scale Variations

There are several occasions when the plasma was found to vary over a very short time scale. For example, saturated spectra were found for all three cups of the main sensor at 0937, when the magnitude of the single spectral peak was decreasing. Comparison of several spectra before and after 0937 UT suggests that if this anomalous spectrum was due to a variation in plasma flow, then the major perturbation lasted for  $\leq 100$  s. There was also a considerable change in the character of the spectra as discussed above.

If it was a feature corotating with the surrounding plasma, then this limited duration converts to a spatial scale of  $\sim 5000$

TABLE 2. Regions of the Torus

|                          | Time  |      | $R, R_J$    | $\lambda$ III, deg | $L$ Shell |        | $n_e, \text{cm}^{-3}$         | Experiment* |
|--------------------------|-------|------|-------------|--------------------|-----------|--------|-------------------------------|-------------|
|                          | UT    | LT   |             |                    | Centered  | Offset |                               |             |
| Outer boundary           |       |      |             |                    |           |        |                               |             |
| Inbound                  | 0630  | 1500 | 7.7         | 128                | 7.7       | 7.6    |                               |             |
| Outbound                 | ~1700 | 2400 | 7.2         | 15                 | 7.5       | 7.5    |                               |             |
|                          |       |      | <i>Warm</i> |                    |           |        |                               |             |
| Peak 1 (warm)            |       |      |             |                    |           |        |                               |             |
| Inbound                  | 0902  | 1445 | 5.90        | 197                | 5.94      | 5.87   | 2160<br>2170                  | PLS<br>PRA  |
| Outbound                 | 1445  | 2245 | 5.70        | 317                | 5.79      | 5.89   | $1500 \pm 50^\dagger$<br>1650 | PLS<br>PRA  |
| Peak 2 (warm)            |       |      |             |                    |           |        |                               |             |
| Inbound                  | 0924  | 1600 | 5.69        | 206                | 5.72      | 5.66   | 3130<br>3500                  | PLS<br>PRA  |
| Outbound                 | 1420  | 2200 | 5.49        | 307                | 5.55      | 5.64   | $1600 \pm 50^\dagger$<br>1950 | PLS<br>PRA  |
| Transition region (cold) |       |      |             |                    |           |        |                               |             |
| Inbound                  | 0945  | 1630 | 5.5         | 215                | 5.5       | 5.5    |                               |             |
| Outbound                 | 1400  | 2210 | 5.3         | 300                | 5.4       | 5.5    |                               |             |
|                          |       |      | <i>Cold</i> |                    |           |        |                               |             |
| Peak 3,                  |       |      |             |                    |           |        |                               |             |
| Inbound (cold)           | 1016  | 1730 | 5.27        | 225                | 5.27      | 5.28   | 1740<br>1750                  | PLS<br>PRA  |

\*PLS Voyager 1 Plasma Science experiment. PRA, Voyager 1 Planetary Radio Astronomy experiment.

†Predicted by model of torus from measurements on the inbound leg of the trajectory.

km. The plasma was a little cooler just before and after the saturated spectrum, as a second spectral peak was briefly discernible. While it is conceivable that a blob of newly ionized material oscillating about the centrifugal equator [Cummings *et al.*, 1980] could have saturated the instrument, the sharp change in the high-energy tail in the spectrum at this time suggests the existence of a physical boundary. The transition region between the inner and outer regions of the torus and the changes in relative abundance of different ions in the in-

ner torus are additional examples of radical changes in the plasma over spatial scales of the order of  $10^4$  km.

#### Phase Space Density

To investigate the nature of diffusive transport of plasma, an estimate of phase space density has been calculated [Bagenal *et al.*, 1980; Richardson *et al.*, 1980]. Figure 13 is a plot of the total number of ions in a unit  $L$  shell times  $L^2$  (i.e.,  $NL^2$ ) against radial distance from Jupiter. This figure shows that the total flux tube content had a maximum at  $\sim 5.7 R_J$  and decreased monotonically radially inward from the peak. Although the charge density at the centrifugal equator has three local maxima at different radial distances, this single peak in the total content of a flux tube suggests transport by diffusion of plasma from a single source near Io [Richardson *et al.*, 1980; Richardson and Siscoe, this issue]. Outside  $\sim 5.7 R_J$  the flux tube content decreased more gradually with distance except around  $7.5 R_J$ , where the total number of ions dropped sharply at the outer edge of the torus. The rapid variations in the flux tube content at  $\sim 5.7$  and  $\sim 7.5 R_J$  probably indicate that radical changes in the diffusive transport of plasma occur at these  $L$  shells. Finally, small-scale ( $10^4$  km) fluctuations in plasma parameters may be evidence of a flux tube interchange diffusion mechanism driven either by turbulence in Jupiter's atmosphere or the instability of magnetic field lines 'loaded' with heavy ions in a centrifugal potential [Siscoe and Summers, this issue].

#### Composition

Figure 14 presents contour maps of the densities of the major ionic species observed in the inner magnetosphere. The maps have been constructed in the same manner as Figure 11 by taking the measurements made on the spacecraft trajectory and extrapolating them along dipolar field lines. The four panels on the left (Figures 14a(i)–14a(iv)) are for the isothermal model. The maps on the right (Figures 14b(i)–14b(iv))

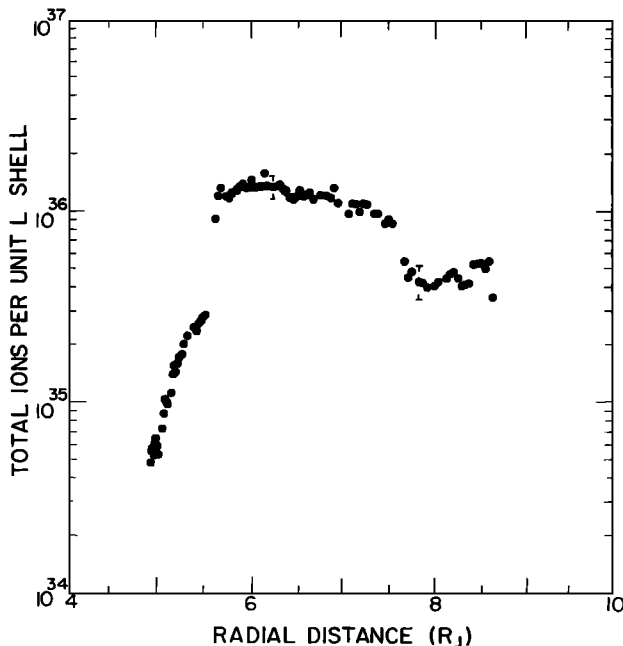


Fig. 13. Radial profile of the total number of ions per unit  $L$  shell constructed from in situ plasma measurements, assuming a dipole magnetic field and a simple exponential scale height distribution for the ions along the field lines. The uncertainties due to thermal-model dependencies are shown by the vertical bars.

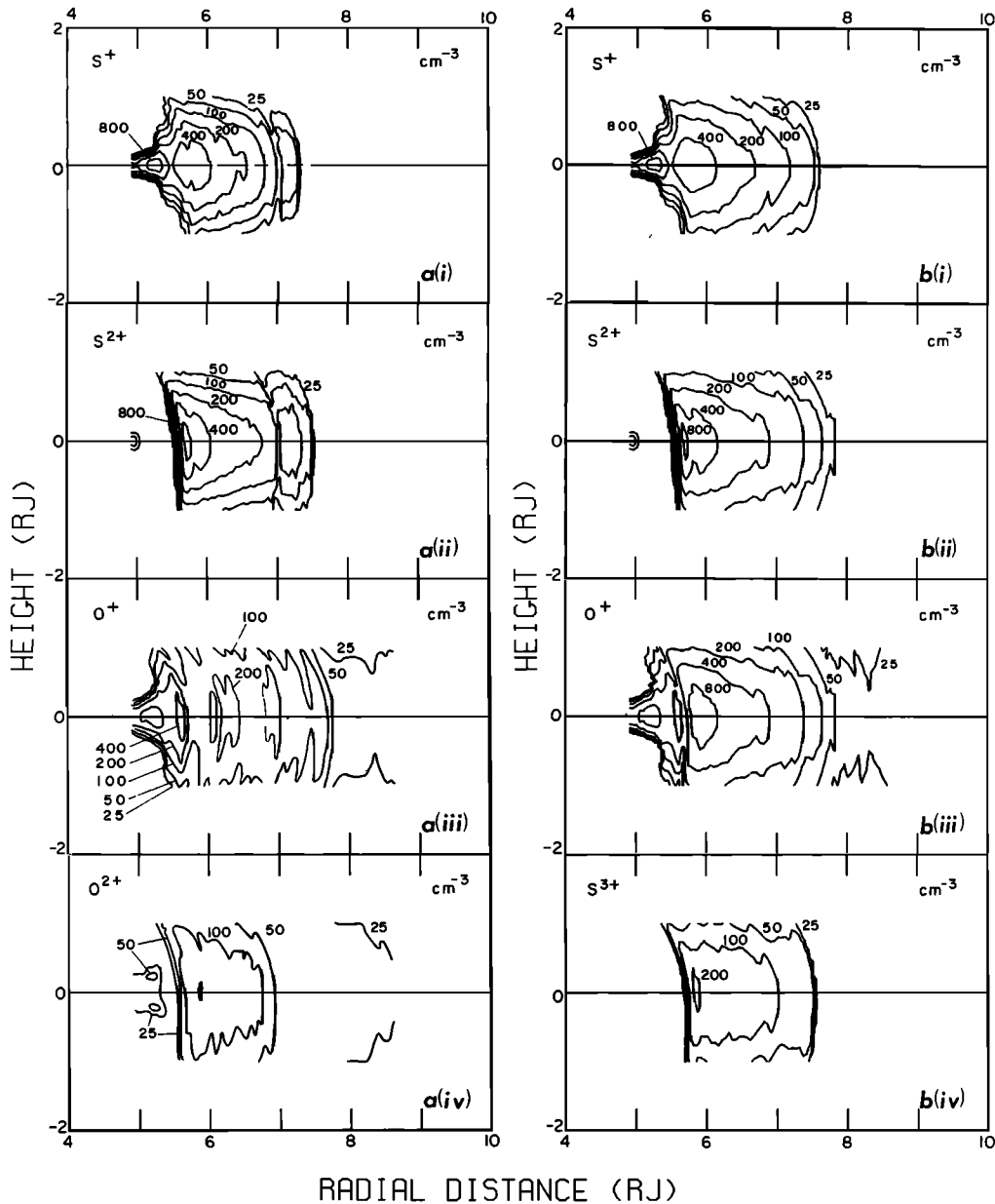


Fig. 14. Contour maps of ion number density for the major ionic species found in the inner magnetosphere of Jupiter. (a) Constructed from fits to the energy per charge spectra assuming the ions have the same temperature. (b) Similarly constructed assuming the ions to be isothermal inside  $L = 5.7$  and to have a common thermal speed at larger  $L$  shells.

have been made using parameters from a fit to the data assuming the ions have the same temperature inside an  $L$  shell of 5.7 and have a common thermal speed outside  $L = 5.7$ . Table 1 gives the composition at the spacecraft location for various radial distances. Table 3 gives the corresponding bulk plasma properties.

The inner (cold) torus region seems to be very strongly dominated by ions with  $A/Z^* = 32$  which are probably singly ionized sulphur. Table 1 shows a density of  $1120 \text{ cm}^{-3}$  for  $\text{S}^+$  which was measured in the center of the inner torus at  $5.3 R_J$ , near the centrifugal equator (see Figure 14a(i) or b(i)). With the  $A/Z^* = 16$  spectral peak being largely  $\text{O}^+$  rather than  $\text{S}^{2+}$  and the absence of  $\text{S}^{3+}$  ( $< 3 \text{ cm}^{-3}$ ), the average charge state of the ions ( $Z_i^*$  of Table 3) is close to unity in this region. The predominance of sulphur is reflected in the average ion mass

number  $\bar{A}_i$  of 28 and a value of 3 for the ratio of the total number of sulphur ions to the total number of oxygen ions ( $\text{S}/\text{O}$ ) at  $5.3 R_J$  (Table 3).

Figure 14a(iv) illustrates how at  $5.3 R_J$ , the minor quantity of doubly ionized oxygen present has been drawn away from the equator by the field-aligned polarization electric field that has been set up by the predominant heavy sulphur ions which are held close to the equator by centrifugal forces. The electrons are too light to be affected much by centrifugal forces so they are only constrained by electrostatic interaction with the ions. Lighter ions of higher charge state are more easily pulled off the centrifugal equator with the electrons so their density distribution along the field lines has a larger effective scale height (the  $\text{O}^+$  torus is thicker than that of  $\text{S}^+$ ). In a more extreme case, sufficient  $\text{O}^{2+}$  ions have been drawn along the

TABLE 3. Bulk Properties of the Plasma

|                          | March 5                |                       |                       |                       |                        | March 4              |                      | March 3,             |       |
|--------------------------|------------------------|-----------------------|-----------------------|-----------------------|------------------------|----------------------|----------------------|----------------------|-------|
|                          | 1120 UT,<br>4.96 $R_J$ | 1016 UT,<br>5.3 $R_J$ | 0859 UT,<br>6.0 $R_J$ | 0527 UT,<br>8.6 $R_J$ | 0150 UT,<br>11.6 $R_J$ | 1550 UT,<br>20 $R_J$ | 0505 UT,<br>28 $R_J$ | 1031 UT,<br>42 $R_J$ |       |
| $n_e$ , cm <sup>-3</sup> | 500                    | 1700                  | 1900                  | 111                   | 111                    | 16.1                 | 1.63                 | 0.73                 | 0.46  |
| $N_n$ , cm <sup>-3</sup> | 431                    | 1630                  | 1300                  | 75                    | 74                     | 11.2                 | 0.96*                | 0.43*                | 0.25* |
|                          |                        |                       | 1200*                 | 61*                   | 64*                    |                      | 1.3†                 | 0.60†                | 0.35† |
|                          |                        |                       | 1760†                 | 77†                   | 77†                    |                      |                      |                      |       |
| $\bar{Z}_i^*$            | 1.1                    | 1.0                   | 1.4                   | 1.5                   | 1.5                    | 1.4                  | 1.7*                 | 1.7*                 | 1.8*  |
|                          |                        |                       | 1.7*                  | 1.7*                  | 1.7*                   |                      | 1.2†                 | 1.2†                 | 1.3†  |
|                          |                        |                       | 1.2†                  | 1.3†                  | 1.4†                   |                      |                      |                      |       |
| $T_{en}$ , eV            |                        |                       | 5.0                   | 10                    | 10                     | 11                   | 20                   | 24                   |       |
| $\bar{T}_n$ , eV         | 0.5                    | 1.1                   | 28                    | 37                    | 28                     | 21                   | 10*                  | 24*                  | 21*   |
|                          |                        |                       | 38*                   | 72*                   | 65*                    | 6.7†                 | 18†                  | 14†                  |       |
|                          |                        |                       | 26†                   | 60†                   | 54†                    |                      |                      |                      |       |
| $\bar{A}_i$              | 21                     | 28                    | 29                    | 22                    | 25                     | 21                   | 23*                  | 25*                  | 22*   |
|                          |                        |                       | 32*                   | 29*                   | 34*                    | 16†                  | 18                   | 16†                  |       |
|                          |                        |                       | 22†                   | 23†                   | 24†                    |                      |                      |                      |       |
| S/O                      | 1                      | 3                     | 3                     | 0.1                   | 2                      | 0.9                  | 5.*                  | 2.*                  | 4.*   |
|                          |                        |                       | 0.6†                  | 1*                    | 5*                     | 0.2†                 | 0.2†                 | 0.2†                 |       |
|                          |                        |                       |                       | 6†                    | 1†                     |                      |                      |                      |       |
| $V/V_c$                  | 1                      | 1                     | 1                     | 0.90                  | 0.77                   | 0.76                 | 0.49                 | 0.43                 |       |

All numbers are derived from plasma parameters obtained using the isothermal model for the ions unless otherwise indicated.

\*From constant thermal speed model when  $A/Z^* = 16$  spectral peak is assumed to be all  $S^{2+}$ .

†From constant thermal speed model when  $A/Z^* = 16$  spectral peak is assumed to be all  $O^+$ .

field lines to form double maxima in their density distribution approximately 0.2  $R_J$  away from the centrifugal equator.

The predominance of heavy ions with lower ionization state near the centrifugal equator means that the composition measured there is not typical of the whole of the torus. The average ion mass number  $\bar{A}_i$  and charge state  $\bar{Z}_i^*$  decrease and increase, respectively, with distance from the centrifugal equator. Similarly, the S/O ratio decreases off the equator so that a summation of the ion densities along the 5.3  $L$  shell suggests a value of  $\sim 2.4$  for the ratio of the total amounts of sulphur and oxygen ions in the inner torus.

In the outer (warm) torus the composition varies according to which thermal model is chosen. The isothermal model produces a composition (illustrated by the contour maps on the left of Figure 14) that is dominated by sulphur with comparable quantities of sulphur ions in the first and second ionization states (though there is little  $S^{3+}$ ). At 6.0  $R_J$ ,  $S^+$  and  $S^{2+}$  ions composed 65% of the measured ion density, but because of their large effective scale heights,  $O^+$  and  $O^{2+}$  become increasingly more important off the equator and dominate the composition at a height of  $\pm 0.8 R_J$ . Therefore when the ion densities are integrated along the  $L = 6.0$  field line, the ratio of the amounts of sulphur and oxygen ions decreases from the in situ value of 5.3 to 2.0. Similarly, the average mass number  $\bar{A}_i$  will be less than 28 and the average charge state  $\bar{Z}_i^*$  greater than 1.5 when taken for a column through the torus instead of at the spacecraft location at 6.0  $R_J$  near the centrifugal equator.

With the common thermal speed model the composition strongly depends on the relative proportions of  $O^+$  and  $S^{2+}$  contributing to the  $A/Z^* = 16$  spectral peak which cannot be determined from fits to the spectra. Figures 14b(ii) and 14b(iii) show the extreme case of only one of the two species being present. If there is no  $O^+$ , then the outer (warm) torus would be totally dominated by sulphur for this model because the lower shoulder in the energy per charge spectra is predominantly  $S^{3+}$  rather than  $O^{2+}$  (see Figure 4 and Table 1 for example at 6.0  $R_J$ ). On the other hand, if there is no  $S^{2+}$  (which seems unlikely if  $S^{3+}$  and  $S^+$  are present), then  $O^+$  be-

comes by far the dominant ion, and the sulphur to oxygen abundance ratio is reduced to 0.6.

The effective scale height for the distribution of ions away from the equator is mainly dependent on their thermal speed with a weaker dependence on charge state. This means for the constant thermal speed model the composition is roughly constant along field lines so that the in situ values of  $\bar{Z}_i^*$ ,  $\bar{A}_i$ , and S/O given in Table 3 for 6.0  $R_J$  are probably fairly typical of the whole of the outer torus. The values of  $\bar{Z}_i^*$  and  $\bar{A}_i$  reflect the change in S/O when either  $S^{2+}$  or  $O^+$  is removed.  $\bar{A}_i$  is reduced from 32 to 22 when  $S^{2+}$  is replaced by  $O^+$ . In the same way  $\bar{Z}_i^*$  decreases from 1.7 to 1.2. These ranges in the values of S/O,  $\bar{A}_i$ , and  $\bar{Z}_i^*$  include the corresponding numbers for the isothermal model at 6.0  $R_J$ .

Outside the torus at 8.6  $R_J$ , setting the plasma flow speed at 90% of the corotational value produces a composition similar to that found inside the torus. If the plasma was strictly corotating, then oxygen would have dominated the composition with an S/O ratio of  $\leq 1$  for all thermal models. Setting the plasma flow speed at 90% of the corotational value changes the composition (Table 1) by more than doubling the amount of  $S^+$ , including more  $S^{3+}$ , and reducing the density of  $O^{2+}$ . The relative proportions of the different ionic species then become more typical of the source region at 6.0  $R_J$  with similar values of S/O,  $\bar{A}_i$ , and  $\bar{Z}_i^*$  for the corresponding thermal models.

The composition in the middle magnetosphere plasma sheet (20–42  $R_J$ ) again depends on the identification of the ionic species that is responsible for the dominant  $A/Z^* = 16$  spectral peak. If the proportion of  $O^+$  and  $S^{2+}$  remains constant with distance, then the composition as a whole is uniform in the plasma sheet. For the two extreme cases of either  $O^+$  or  $S^{2+}$  dominating the composition,  $\bar{A}_i$  would have a value of 19 or 30, while  $\bar{Z}_i^*$  would be either 1.2 or 2.0.

#### Alfven Speed

As mentioned above, the total mass density of the plasma is determined from positive ion energy per charge spectra independent of assumptions of composition. The mass density

measurements ( $\rho$ ) can be combined with the magnitude of the magnetic field ( $B$ ) to calculate a local Alfvén speed ( $V_A = B / (4\pi\rho)^{1/2}$ ). At each point, the magnitude of the magnetic field has been determined from the Pioneer 04 model of *Acuña and Ness* [1976]. Figure 15 shows a contour map of local Alfvén speed, constructed in a fashion similar to those in Figures 12 and 14. A dipolar magnetic field geometry has been used to extrapolate the in situ plasma measurements and hence determine the local mass density at different points along a field line. The resulting local Alfvén speed is uniformly low in the outer torus with minimum values of  $\approx 250$  km s<sup>-1</sup> near the centrifugal equator. Above and below the torus the rapidly decreasing density and larger magnetic field produce a rapid increase in Alfvén speed. Io orbits Jupiter in a plane normal to the Jovian rotation axis but at a rate slower than the planetary rotation rate, so that the position of the satellite with respect to the centrifugal equator varies as shown in Figure 15. The Alfvén speed of the plasma in the vicinity of Io therefore varies by a factor of 2 with the System III longitude of the satellite.

The perturbations of magnetic field and plasma flow measured when the Voyager 1 spacecraft passed beneath Io suggest that a standing Alfvén wave is generated near Io, making a current system connecting Io and the ionosphere of Jupiter [*Acuña et al.*, this issue; *Belcher et al.*, this issue]. The large Alfvén speeds outside the torus mean that the time for Alfvén waves generated near Io to reach the ionosphere is largely determined by the length of the propagation path in the torus. This transit time will therefore be strongly modulated by the System III position of Io. Similarly, other properties of the propagating waves such as geometry and damping will also vary with longitude. The subsequent changes in the field-aligned current associated with the Alfvén wave may explain the Io modulation of the decametric radiation [*Gurnett and Goertz*, 1981].

#### DISCUSSION

The direct plasma measurements presented here describe the basic structure of the torus. The next task is to use this information of the thermal state and spatial distribution to investigate the nature of the source, transport mechanisms and energy balance of the plasma.

Although the source for torus plasma appears to be Io, it is not clear exactly where the ionization takes place. The high-energy cutoff observed in spectra inside  $5.7 R_J$ , the existence of an extensive cloud of neutral sodium atoms, and the recent observations of neutral oxygen [*Brown*, 1980] near Io suggest that the sulphur and oxygen ions may come from clouds of neutral atoms. When picked up by the magnetic field, the freshly ionized particles would gain a gyro speed equal to the magnitude of the difference between the neutral atoms' original velocity and the local corotation velocity. At  $6 R_J$ , sulphur and oxygen ions would gain gyro energies of  $\sim 545$  and  $\sim 270$  eV, respectively. Most of this energy would have to be removed from the ions to produce the observed temperatures of less than 30 eV for the bulk of the plasma.

An alternative source mechanism could explain the low temperatures measured in the torus by producing ions which pick up smaller gyro energies. This would happen if the ionization occurred close to Io, where currents generated in the complicated interaction of the magnetospheric plasma with the satellite reduced the local corotational electric field [*Goertz*, 1980]. The problem with such a localized source mechanism is that the Voyager ultraviolet measurements in-

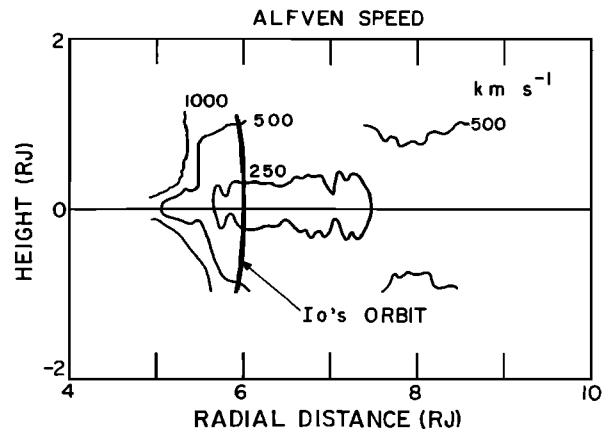


Fig. 15. Contour map of local Alfvén speed calculated from the 04 magnetic field model [*Acuña and Ness*, 1976] and the total ion mass density, measured on the spacecraft trajectory and extrapolated along the field lines.

indicated that there was no enhancement of emission in the vicinity of Io [*Shemansky*, 1980]. Similarly, any neutral clouds would have to be more extensive than the sodium cloud unless the freshly ionized material composes a small fraction of the total plasma in the torus. A localized source region would also be feasible if the initial source material was an ion such as  $\text{SO}_2^+$  which does not generally emit at ultraviolet wavelengths and could subsequently dissociate further away from Io to produce the observed ionic species.

The detection of an  $\text{SO}_2$  atmosphere by *Pearl et al.* [1979] and  $\text{SO}_2$  frost on the surface of Io [*Fanale et al.*, 1979; *Smythe et al.*, 1979] makes  $\text{SO}_2$  an obvious source material for the plasma torus. The characteristics of the dissociation and ionization processes for  $\text{SO}_2$  are not well known. However, *Shemansky* [1980] and *Kumar* [1979] suggest they probably involve  $\text{O}_2$  and  $\text{SO}$  molecules and their ions, especially on the nightside of Io, where  $\text{O}_2$  may dominate the atmosphere [*Kumar and Hunten*, 1980]. The existence of intermediate dissociation products as well as the fact that oxygen is less readily ionized than sulphur may explain why more sulphur was observed in the torus than expected from the full dissociation and ionization of  $\text{SO}_2$ . On the other hand, there is probably a significant amount of elemental sulphur on the surface of Io [*Masursky et al.*, 1979]. There must be some mechanism such as sputtering for removing from Io material which is not a major constituent of the atmosphere because neutral sodium has been observed in the vicinity of Io for many years and sodium ions have been detected in the magnetosphere [*Krimigis et al.* 1979; *Vogt et al.* 1979; *Sullivan and Bagenal*, 1979]. Therefore additional sulphur may be supplied to the torus by a similar process.

The Voyager I ultraviolet spectrometer (UVS) detected emission at wavelengths associated with spectral lines of  $\text{S}^{2+}$ ,  $\text{S}^{3+}$ ,  $\text{O}^{2+}$  and  $\text{O}^+$  ions [*Broadfoot et al.*, 1979; *Sandel et al.*, 1979]. By comparing emission strengths at different spectral lines it is possible to estimate the densities of the emitting ions as well as put limits on the densities of ions with spectral lines at wavelengths where the emission was low. Unfortunately, the spectrometer does not have sufficient resolution to distinguish between some of the spectral lines which are found at similar wavelengths but correspond to different ionic species. At the present levels of uncertainty in both the UVS and plasma determinations of the densities of different ions the two measurements of composition are consistent [*Shemansky*,

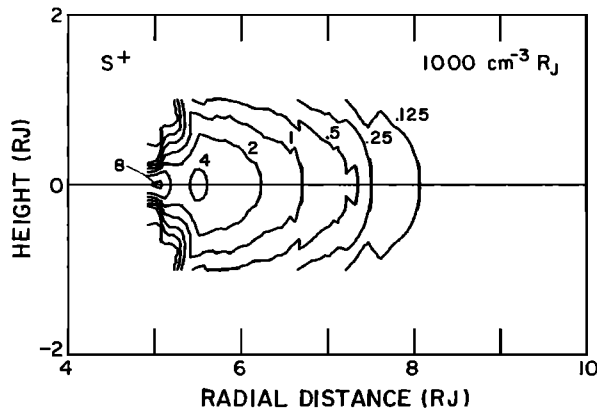


Fig. 16. Contour map of the column density of  $S^+$  ions constructed using the constant thermal speed model and assuming that the plasma is azimuthally symmetric at any constant distance from the centrifugal equator. The local density is then integrated along a line of sight perpendicular to the rotation axis in a plane containing the magnetic dipole to produce a column density through the torus.

1980]. However, the UVS results generally suggest there were more  $O^{2+}$  and  $S^{3+}$  ions but less  $S^+$  than inferred by the plasma instrument in the warm torus (for both thermal models).

There are several important factors involved when the remotely observed emission intensities are compared with in situ density measurements. The plasma electrons which collisionally excite the emitting ions have at least two components to their energy distribution [Scudder *et al.*, this issue], making the inference of plasma parameters from emission strengths much more complicated. A more straightforward problem is that of geometry. All remote observations are integrals of emission along a line of sight from the detector through the torus. The in situ plasma measurements suggest the plasma properties vary considerably along such a line. However, the torus appears to be optically thin so that most of the emission comes from the section of the line with the highest density. If the aperture of the detector is a slit, then spatial resolution may be lost in the direction of the length of the slit. This is a particular problem with the Voyager ultraviolet observations, where the slit was generally aligned with the rotation axis of Jupiter and covered a strip which was  $0.25 R_J$  long at best and generally much longer. Therefore the densities calculated from ultraviolet emission for a torus thickness of  $2 R_J$  underestimate the amount of  $S^+$  which is more closely confined to the equator [Strobel, 1980].

Pilcher and Morgan [1980] have produced images of the  $S^+$  emission which show the distribution of plasma in both radial and latitudinal directions. Peak intensities come from regions around 5 and  $5.5 R_J$  on the centrifugal equator which match the positions of the maximum column densities calculated from the in situ measurements shown in Figure 16. The column density has been calculated assuming the plasma is uniformly distributed around Jupiter at constant distances from the planet and from the centrifugal equator. Although the locations of the density maxima are closer to Jupiter when the local density is integrated along a line (because of torus geometry), there remains a considerable quantity of sulphur outside  $6 R_J$  which is not seen in the data of Pilcher and Morgan [1980]. Although molecular ions have small lifetimes against dissociation, this may be evidence of the presence of  $O_2^+$  or  $SO_2^{2+}$  which cannot be distinguished from  $S^+$  in the plasma

data. On the other hand, it may just reflect radial changes in the electron properties [Scudder *et al.*, this issue].

The 'wedge' shape of the emitting  $S^+$  cloud illustrated by the images of Pilcher and Morgan [1980] and deduced from earlier observations [Nash, 1979] indicate the temperature transition from the warm torus to the cold torus. In fact, plasma temperatures as low as  $\sim 2$  eV and densities of  $3000 \text{ cm}^{-3}$  were predicted from the ground-based optical measurements as early as 1976 [Brown, 1976]. The  $O^+$  emission observed by Pilcher and Morgan [1980] came from a region which is extended further away from the centrifugal equator than the region of sulphur emission. This is consistent with the ions having a similar temperature so that the oxygen ions have a larger effective scale height. However, the UVS observation show no variation in the relative densities of  $S^{3+}:S^{2+}:O^{2+}$  with latitude, which may reflect either different source regions for the optical and ultraviolet emissions or a variation in plasma conditions with time [Broadfoot *et al.*, 1979; Sandel *et al.*, 1979].

Although the spatial resolution of ground-based measurements is currently limited, monitoring large-scale spatial structure such as the variation of plasma properties with local time, system III longitude, or the location of Io may clarify the importance of magnetic field asymmetries [Dessler and Hill, 1979] and the nature of Io's interaction with the magnetospheric plasma. Similarly, the variation of plasma properties with time determined from ground-based studies is very important for investigations of the nature of the source and for studies of the diffusion and energy balance of the plasma torus [Brown, 1976; Mekler and Eviatar, 1980].

To explain the radial temperature profile that is observed, it is necessary to consider the many factors in the total energy balance of the torus. The sources of energy are largely the newly ionized material as well as any currents or wave/particle interactions in the torus or inwardly diffusing energetic particles. Energy is removed from the torus by radiation (ultraviolet, optical, and radio), particle loss (precipitation into the ionosphere of Jupiter or to a small extent recombination), and transport into other parts of the magnetosphere via particle diffusion. Therefore the main task of solving the energy balance for the torus plasma involves finding source and diffusion mechanisms which are consistent with the emitted radiation and observed plasma temperature as well as providing the correct mass to load the middle magnetosphere and slow down its rotation. To add to the complexity of the situation, all of these processes probably vary considerably with time, so it is not clear that a steady state description is realistic.

However, a scenario may be postulated to explain the distinct separation of the Io plasma torus into an inner (cold) region and an outer (warm) region. If the fraction of ions produced near Io which diffuses outward is considerably larger than the fraction which diffuses inward [Richardson and Siscoe, this issue; Siscoe and Summers, this issue], then the few inwardly diffusing particles are transported slowly and so have time to cool by radiation. As the plasma cools, it becomes more confined to the centrifugal equator. The resulting increase in the local density enhances the emission so that the plasma cools further. The combination of cooling and increased density possibly leads to a significant loss of ions by recombination. This runaway process would result in a sharp transition region between the regions of inward and outward diffusion. The plasma that rapidly diffuses outward does not have time to cool by radiation. The fact that the temperature

does not decrease with distance suggests that the expected adiabatic cooling must be largely balanced by a heat source in the outer torus. Another consideration may be that the processes that accelerate particles in the middle and outer magnetosphere may also operate closer in toward Jupiter, maintaining a more uniform temperature in the outer torus.

The suggestion of *Cummings et al.* [1980] for the observed spatial structure in the density profile as being due to latitudinally oscillating plasma blobs and a commalike region near Io does not account for the observed symmetry between the location of the inbound and outbound peaks and boundaries or the observed thermal profile. If the pickup of neutrals is the major source mechanism (as the observations might suggest), then the very localized source region proposed by *Cummings et al.* [1980] would appear to conflict with the diffuse nature of the neutral clouds.

### CONCLUSIONS

There are places in the inner magnetosphere such as the inner (cold) torus region where the Voyager 1 plasma measurements define the composition, density, temperature, distribution, and dynamics of the plasma during the spacecraft flyby on March 5, 1979. In the remaining regions these quantities are not all uniquely determined, so it has been necessary to construct models based on the available data. A range of plasma parameters for the Io plasma torus has been determined from the data and is presented in this paper. These parameters can be tested to see if they are consistent with both direct observations of the electron number density by other instruments on the same spacecraft and indirect determinations of quantities such as the source strength, diffusion rates, the emission and propagation of electromagnetic waves, etc. There is a great wealth of information from the Voyager 1 traversal of the inner magnetosphere which has by no means been fully tapped. The analysis of the plasma data alone is far from exhaustive, and the picture of the Io plasma torus should eventually be much clearer when the clues from different observations are put together.

The main features of the inner magnetosphere that have been determined from the Voyager plasma measurements are the following:

1. There are two distinct regions of plasma torus. In the inner part ( $<5.5 R_J$ ) the cold ( $<1$  eV) plasma is closely confined to the centrifugal equator (density scale height of  $\sim 0.2 R_J$ ), and the ions appear to be isothermal. Between ( $5.5$  to  $7.5 R_J$ ) the plasma is warm ( $\sim 30$  eV) and forms a thick torus near the centrifugal equator (density scale height  $\sim 1 R_J$ ). Most of the electrons are a factor of 3 to 5 colder than the ions in this outer region.

2. The transition region between the two parts of the torus is very narrow ( $\pm 0.1 R_J$  at  $5.5 R_J$ ). In this region the plasma temperature has a very steep gradient of  $\sim 7 \times 10^5$  K  $R_J^{-1}$ . Although the equatorial density of the plasma has a local minimum at  $5.5 R_J$ , the total number of ions in a flux tube does not. The flux tube content decreases on either side of the single source region near Io's orbit with a much steeper gradient inward than away from Jupiter.

3. The outer edge of the torus at  $7.5 R_J$  is probably where the plasma ceases strictly to corotate with Jupiter. This may also be the region where the flux tube mass becomes critically loaded with plasma triggering a more efficient mechanism for outward diffusion.

4. The ionic composition of the plasma varies rapidly with

radial distance throughout the torus and particularly inside  $5.7 R_J$ . This is in contrast to the plasma sheets in the middle magnetosphere which have a fairly constant composition over a large radial distance ( $20$ – $42 R_J$ ). In the torus the composition is dominated by sulphur unless  $O_2^+$  is a major constituent. The dominance of sulphur is inconsistent with the complete dissociation and ionization of  $SO_2$ .

5. The kinetic temperature of the bulk of the plasma throughout the torus is well below that expected if the ions were picked up by the magnetic field and had retained gyro-speeds equal to the speed of corotation. However, there is evidence that a small fraction of the ions do have energies corresponding to the full corotational value.

6. The large mass density of the plasma in the torus produces a region where the Alfvén speed is uniformly low ( $<250$  km  $s^{-1}$ ) surrounded by regions of much higher Alfvén speed.

### APPENDIX: THE DISTRIBUTION OF PLASMA ALONG MAGNETIC FIELD LINES

To determine the variation of plasma density along a magnetic field line in the Io plasma torus, several simplifying assumptions have been made. First of all, the system is taken to be in a steady state, since the characteristic time scale for diffusion is of the order of several days, while typical bounce periods range from seconds for electrons to a few hours for cold, heavy ions. Forces due to Coulomb collisions have also been ignored because except in the coldest and densest part of the torus, collisions are relatively infrequent. The electron population has been split into two components: a predominant one of cold thermal electrons and the other a minor proportion of hot electrons. These two components are treated separately, and any coupling that must occur between them is taken to be negligible. This steady state picture also ignores any loss of particles due to precipitation into the ionosphere of Jupiter. Such an assumption is probably reasonable in this case except for the hot electrons, which may have a significant loss cone.

With the above assumptions the variation of plasma density along a magnetic field line is determined by the equilibrium pressure gradient which balances the combined forces of gravitation, centrifugal acceleration, and a polarization electric field for all electrons and ions. The equation for the balance of field-aligned forces for each electron component is

$$-\frac{dP_e}{ds} = -m_e n_e f + n_e q E \quad (1)$$

and for each ionic species there is a similar equation,

$$-\frac{dP_i}{ds} = -m_i n_i f - Z_i^* n_i q E \quad (2)$$

where  $P_e$  and  $P_i$  are the partial pressures of the electrons and each ionic species ( $i$ );  $m_e$ ,  $m_i$ ,  $n_e$ ,  $n_i$ ,  $Z_i^*$  correspond to mass, number density, and charge state;  $s$  is the distance along the field line;  $f$  is the 'gravitational' term which includes the effects of centrifugal acceleration and can be determined for the simple geometry of a dipole magnetic field.

These two sets of equations are coupled by the preservation of local charge neutrality,

$$n_e^{\text{hot}} + n_e^{\text{cold}} = \sum_i Z_i^* n_i \quad (3)$$

To discuss the properties of these expressions, it is helpful to consider the history of their application to magnetospheric

studies. *Angerami and Thomas* [1964] took a single electron component, assumed the ideal gas law, and set  $T_e/T_i$  to be constant along each field line, so (3) became

$$\frac{dP_e}{T_e} = \sum_i \frac{Z_i^* dP_i}{T_i} \quad (4)$$

They then used (4) to couple (1) and (2) and hence relate the parallel electric field  $E$  to the gravitational term:

$$qE = \frac{\left( \sum_i m_i n_i Z_i^* C_i - m_e n_e \right)'}{\sum_i n_i Z_i^* C_i + n_e} = m^+ f \quad (5)$$

where  $C_i = T_e/T_i$  and  $m^+$  is the effective ('temperature weighted') ion mass. (For a single-ion species and  $C_i = 1$ ,  $m^+$  is simply  $m_i/(Z_i^* + 1)$ .) Substituting (5) back into (1) and (2) and integrating along the field line yield

$$\frac{n_e(s)T_e(s)}{n_e(s_0)T_e(s_0)} \exp \left[ - \int_{s_0}^s \frac{m^+}{kT_e} f ds' \right] \quad (6)$$

$$\frac{n_i(s)T_i(s)}{n_i(s_0)T_i(s_0)} = \exp \left[ - \int_{s_0}^s \frac{(m_i - Z_i^* m^+)}{kT_i} f ds' \right] \quad (7)$$

*Angerami and Thomas* [1964] used various models of temperature to solve (6) and (7) to determine the distribution of plasma from the earth's ionosphere and away from the planet along dipolar magnetic field lines.

*Gledhill* [1967] was the first to apply these expressions to Jupiter's magnetosphere. He showed that because of Jupiter's rapid rotation the centrifugal contribution will dominate the gravitational force so that a plasma with a single ionic species will find an equilibrium position at the furthest point along the field line from the rotational axis of the planet. *Gledhill* also noted that because of the  $10^\circ$  tilt of the magnetic axis with respect to the rotation axis, the equilibrium position is on a surface between the magnetic and rotational equatorial planes. *Hill et al.* [1974] have called this plane the 'centrifugal symmetry surface.' As true gravitational forces can be neglected at distances greater than  $2 R_J$  [*Michel and Sturrock*, 1974], the equilibrium position of the plasma is found where the sum of field-aligned components of the remaining forces become zero [*Siscoe*, 1977]:

$$F = -\mu \frac{\partial B}{\partial s} - m\Omega^2 r \cos(\theta - \alpha) \cos \delta + Z^* qE \quad (8)$$

The first term on the right-hand side of (8) is the magnetic mirror force, where the magnetic moment  $\mu = (mV_g)^2/2B$  ( $V_g$  is the gyro speed,  $\Omega$  the rotation rate of Jupiter,  $r$  the radial distance,  $\delta$  the angle between the rotational equator and the tangent to the local magnetic field, and  $\alpha$  the angle between the rotational and magnetic equatorial planes; see Figure 17). For a dipole geometry the magnetic mirror force can be approximated by

$$F_m = \frac{9}{2} \frac{mV_g^2 \sin \theta}{R_J L \cos^2 \theta} \quad (9)$$

for low magnetic latitudes ( $\theta \lesssim 10^\circ$ ) [*Siscoe*, 1977]. Similarly, the centrifugal force becomes

$$F_c = 3 m\Omega^2 R_J L \cos^2 \theta \cos(\alpha - \theta) \cos \delta \quad (10)$$

The relative importance of these for ions is given by the ratio of the gyro energy  $K_g$  to rotational energy  $K$ :

$$\frac{F_m}{F_c} \sim \frac{3K_g}{2K} = \frac{3V_g^2}{2\Omega^2 L^2 R_J^2} \quad (11)$$

(For full expression, see *Cummings et al.* [1980].) Therefore if the plasma is 'hot' and the gyro energy  $K_g = \frac{1}{2} mV_g^2$  is large, then the equilibrium position will be where  $\sin \theta = 0$ , at the magnetic equator [*Goertz*, 1976]. On the other hand, for cold plasma the magnetic mirror force can be ignored and the equilibrium position is  $\theta_0 \approx \alpha/3$  [*Hill et al.*, 1974]. For the Voyager plasma data analyzed in this paper,  $\frac{3}{2} K_g/K$  has a maximum value at 6.8–7.4  $R_J$  of  $\sim 0.1$  but is well below 0.05 in the rest of the torus. The magnetic mirror force is then negligible, and the centrifugal symmetry surface may be taken to be inclined at  $\alpha/3$  from the magnetic equatorial plane. The magnetic mirror force can also be neglected for electrons because for small variations in latitude ( $\pm 10^\circ$ ) the magnitude of the magnetic field does not change significantly compared with the electrostatic potential:

$$\frac{\Delta B}{B} \ll \frac{\Delta \phi}{T_e} \sim \frac{m_i \Delta f}{2T_e} \quad (12)$$

For the hot component of the electron population the magnetic mirror force is more important. In fact, *Scudder et al.* [this issue] show that in the middle magnetosphere the local density maximum (of the hot component) is nearer the magnetic rather than centrifugal equator. However, it will be illustrated below that in the torus region the hot electrons play a very minor role in the spatial distribution of plasma. Therefore the gravitational term  $f$  is just due to the centrifugal force  $F_c$  (equation (10)) which can now be inserted into the exponent of (6) and (7). These two sets of equations can be solved if the temperatures  $T_e$  and  $T_i$  are known as a function of  $s$ . The simplest case is to arbitrarily assume the temperatures are constant along a field line. This is probably quite a reasonable assumption for a collisionless plasma dominated by the strong centrifugal forces on the heavy ions which vary quite rapidly with distance from the equator. If  $m^+$ ,  $T_e$ , and  $T_i$  are constant along a field line, the exponents in (6) and (7) can be integrated along  $s$ . The result is an exponential scale height solution for the distribution of ions along a field line, in the region of small distance  $z = r \sin \theta$  from the centrifugal symmetry surface:

$$\begin{aligned} \frac{n_i(z)}{n_i(z=0)} &= \exp \left[ - \frac{(m_i - Z_i^* m^+)}{kT_i} \frac{3\Omega^2 z}{2} \right] \\ &= \exp [-(z/H)^2] \end{aligned} \quad (13)$$

[*Hill and Michel*, 1976], where the scale height is  $H = (2kT_i/3m^*\Omega)^{1/2}$ ,  $m^* = (m_i - Z_i^* m^+)$  is the effective mass for the ions (which becomes  $m^* = m^+ = m_i/(Z_i^* + 1)$  for a single-ion species and  $T_i = T_e$ ). The electrons have a similar distribution with  $m^* = m^+$ .

This exponential scale height distribution was used (with  $T_e = T_i$ ) by *Bagenal et al.* [1980] to construct a preliminary model of electron density structure in the torus. However, the validity of the method hinges on the assumption that the effective mass is constant for a given field line. The effective mass will not vary if the composition is constant, i.e., a single ionic species predominates or most of the ions have a similar scale height. This assumption does not hold in the Io plasma torus,

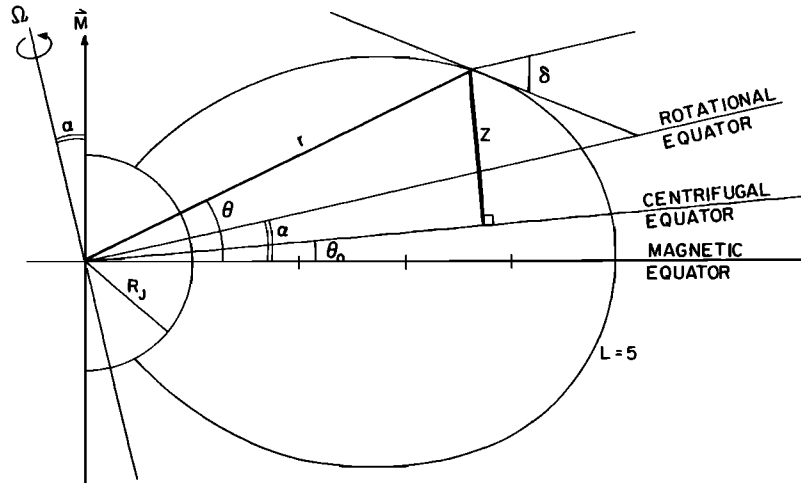


Fig. 17. Geometry of a tilted dipole magnetic field in a meridional plane. The angle between the tangent to the local magnetic field line and the projection of the rotational axis onto the meridional plane is shown by  $\delta$ .

where there are comparable proportions of  $S^+$ ,  $S^{2+}$ ,  $S^{3+}$ ,  $O^+$ , and  $O^{2+}$  with different scale heights. Therefore it was necessary to return to the original equations (1) and (2) to derive the expression for the plasma distribution along the field line without eliminating the electric field. Under the steady state condition the parallel electric field can be expressed as a gradient of an electrostatic potential so that if the temperatures  $T_e$  and  $T_i$  are taken to be constant for a given field line, then (1) and (2) can be integrated over  $s$  to give

$$\frac{n_e(s)}{n_e(s_0)} = \exp \left[ -q \frac{\phi(s) - \phi(s_0)}{kT_e} \right] \quad (14)$$

and

$$\frac{n_i(s)}{n_i(s_0)} = \exp \left[ -\frac{m_i \Omega^2 r^2 \cos^2 \theta}{kT_i^2} + Z^* q \frac{\phi(s) - \phi(s_0)}{kT_i} \right] \quad (15)$$

that is,

$$\int_{s_0}^s f ds = \int_{s_0}^s \Omega^2 r \cos(\theta - \alpha) \cos \delta ds \approx \frac{\Omega^2 r^2}{2} \cos^2 \theta$$

As  $m_e \ll m_i$ , the centrifugal term is neglected for electrons.

In this paper, (14) and (15) have been combined with the condition of charge neutrality (equation (3)),

$$n_e^{\text{hot}} + n_e^{\text{cold}} = \sum_i Z_i^* n_i$$

in an iterative procedure to determine the densities of each ion species  $n_i(s)$  and of the electrons,  $n_e(s)$ , as well as the electrostatic potential  $\phi(s)$ , with respect to a reference point  $s_0$ , the spacecraft location where  $n_i(s_0)$ ,  $n_e(s_0)$ ,  $T_i$ ,  $T_e$  are measured. The values of  $n_i$ ,  $T_i$ , and  $n_e^{\text{hot}} + n_e^{\text{cold}}$  are determined from fits to the positive ion spectral measurements, while  $T_e^{\text{hot}}$ ,  $T_e^{\text{cold}}$ , and  $n_e^{\text{hot}}/n_e^{\text{cold}}$  are determined where possible from the electron measurements. Outside  $\sim 7 R_J$ , the electron parameters are well determined. Between  $5.7$  and  $7 R_J$ , in the warm torus, the spacecraft probably became slightly negatively charged, which at present introduces an uncertainty in the electron measurements (approximately a factor of 3 for  $T_e^{\text{cold}}$ ). The uncertainties in the determination of  $T_e^{\text{hot}}$  and  $n_e^{\text{hot}}/n_e^{\text{cold}}$  are insignificant, as the large value of  $T_e^{\text{hot}}$  makes  $n_e^{\text{hot}}$  almost constant along a field line (see (14)) and because  $n_e^{\text{hot}}/n_e^{\text{cold}}$  has a

value of less than 1% in the torus. All of these uncertainties in the electron parameters have a smaller effect than the uncertainties in  $T_i$ , due to the two different thermal models used in the fit procedure in the warm torus. In the cold torus the electrons were not detected as they were below the energy per charge threshold of the instrument. Therefore inside  $5.7 R_J$  all the electrons were arbitrarily assumed to be at the same temperature as the ions.

*Acknowledgments.* The authors are particularly grateful to Herb Bridge for his assistance throughout this study. The authors thank John Belcher and George Siscoe for extensive advice, Chris Goertz and Stan Olbert for elucidating the plasma physics of the Io torus, and Jack Scudder and Ed Sittler for helpful discussions of the electron data. Jack Connerny, Mario Acuña, and Norman Ness are thanked for discussing the Voyager 1 magnetic field data. The authors would also like to thank Ralph McNutt, Charles Goodrich, Al Lazarus, and other members of the MIT Space Plasma Science Group for their advice and assistance. Work for this paper was supported in part by NASA contract 953733.

## REFERENCES

- Acuña, M. H., and N. F. Ness, The main magnetic field of Jupiter, *J. Geophys. Res.*, **81**, 2917, 1976.
- Acuña, M. H., F. M. Neubauer, and N. F. Ness, Standing Alfvén wave current system at Io: Voyager 1 observations, *J. Geophys. Res.*, this issue.
- Angerami, J. J., and J. O. Thomas, Studies of planetary atmospheres, *J. Geophys. Res.*, **69**, 4537, 1964.
- Bagenal, F., J. D. Sullivan, and G. L. Siscoe, Spatial distribution of plasma in the Io torus, *Geophys. Res. Lett.*, **7**, 41, 1980.
- Belcher, J. W., C. K. Goertz, and H. S. Bridge, The low energy plasma in the Jovian magnetosphere, *Geophys. Res. Lett.*, **7**, 17, 1980.
- Belcher, J. W., C. K. Goertz, J. D. Sullivan, M. H. Acuña, and N. F. Ness, Plasma observations of the Alfvén wave generated by Io, *J. Geophys. Res.*, this issue.
- Birmingham, T. J., J. K. Alexander, M. D. Desch, R. F. Hubbard, and B. M. Pedersen, Observations of electron gyroharmonic waves and the structure of the Io torus, *J. Geophys. Res.*, this issue.
- Bridge, H. S., J. W. Belcher, R. J. Butler, A. J. Lazarus, A. M. Marvetic, J. D. Sullivan, G. L. Siscoe, and V. M. Vasyliunas, The plasma experiment on the 1977 Voyager mission, *Space Sci. Rev.*, **21**, 259, 1977.
- Bridge, H. S., J. W. Belcher, A. J. Lazarus, J. D. Sullivan, R. L. McNutt, F. Bagenal, J. D. Scudder, E. C. Sittler, G. L. Siscoe, V. M. Vasyliunas, C. K. Goertz, and C. M. Yeates, Plasma observations near Jupiter: Initial results from Voyager 1, *Science*, **204**, 987, 1979.

- Broadfoot, A. L., M. J. S. Belton, P. Z. Takacs, B. R. Sandel, D. E. Shemansky, J. B. Holberg, J. M. Ajello, S. K. Atreya, T. M. Donahue, H. W. Moos, J. L. Bertaux, J. E. Blamont, D. F. Strobel, J. C. McConnell, A. Dalgarno, R. Goody, and M. B. McElroy, Extreme ultraviolet observations from Voyager 1 encounter with Jupiter, *Science*, 204, 979, 1979.
- Brown, R. A., I. A. U. Symposium No. 65, presented 1973, in *Exploration of Planetary Systems*, edited by A. Woszczyk and C. Iwaniszewska, p. 527, International Astronomical Union, Torun, Poland, 1974.
- Brown, R. A., A model of Jupiter's sulphur nebula, *Astrophys. J.*, 206, L179, 1976.
- Brown, R. A., The Jupiter hot plasma torus: Observed electron temperature and energy flows, submitted to *Astrophys. J.*, 1980.
- Carlson, R. W., and D. L. Judge, Pioneer 10 ultraviolet photometer observations at Jupiter encounter, *J. Geophys. Res.*, 79, 3623, 1974.
- Cummings, W. D., A. J. Dessler, and T. W. Hill, Latitudinal oscillations of plasma within the Io torus, *J. Geophys. Res.*, 85, 2108, 1980.
- Dessler, A. J., and T. W. Hill, Jovian longitudinal control of Io-related radio emission, *Astrophys. J.*, 227, 664, 1979.
- Fanale, F. P., R. H. Brown, D. P. Cruikshank, and R. N. Clarke, Singificance of absorption features on Io's IR reflectance spectrum, *Nature*, 280, 761, 1979.
- Frank, L. A., K. L. Ackerson, J. H. Wolfe, and J. D. Mihalov, Observations of plasmas in the Jovian magnetosphere, *J. Geophys. Res.*, 81, 457, 1976.
- Gledhill, J. A., Magnetosphere of Jupiter, *Nature*, 214, 155, 1967.
- Goertz, C. K., Plasma in the Jovian magnetosphere, *J. Geophys. Res.*, 81, 2007, 1976.
- Goertz, C. K., Io's interaction with the plasma torus, *J. Geophys. Res.*, 85, 2949, 1980.
- Goertz, C. K., and M. F. Thompson, Radial diffusion of Io-injected plasma, *J. Geophys. Res.*, 84, 1499, 1979.
- Gurnett, D. A., and C. K. Goertz, Multiple Alfvén wave reflections excited by Io: Origin of the Jovian decametric arcs, *J. Geophys. Res.*, 86(A2), 717-722, 1981.
- Gurnett, D. A., R. R. Shaw, R. R. Anderson, and W. S. Kurth, Whistlers observed by Voyager 1: Detection of lightning on Jupiter, *Geophys. Res. Lett.*, 6, 511, 1979.
- Gurnett, D. A., F. L. Scarf, W. S. Kurth, R. R. Shaw, and R. L. Poynter, Determination of Jupiter's electron density profile from plasma wave observations, *J. Geophys. Res.*, this issue.
- Hill, T. W., and F. C. Michel, Heavy ions from the Galilean satellites and the centrifugal distortion of the Jovian magnetosphere, *J. Geophys. Res.*, 81, 4561, 1976.
- Hill, T. W., A. J. Dessler, and F. C. Michel, Configuration of the Jovian magnetosphere, *Geophys. Res. Lett.*, 1, 19, 1974.
- Kaiser, M. L., and M. D. Desch, Narrow-band Jovian kilometric radiation: A new radio component, *Geophys. Res. Lett.*, 7, 389, 1980.
- Krimigis, S. M., T. P. Armstrong, W. I. Axford, C. O. Bostrom, C. Y. Fan, G. Gloeckler, L. J. Lanzerotti, E. P. Keath, R. D. Zwickl, J. F. Carbary, and D. C. Hamilton, Low-energy charged particle environment at Jupiter: A first look, *Science*, 204, 998, 1979.
- Kumar, S., The stability of an SO<sub>2</sub> atmosphere on Io, *Nature*, 280, 758, 1979.
- Kumar, S., and D. M. Hunten, The atmospheres of Io and other satellites, in *The Satellites of Jupiter*, University of Arizona Press, Tucson, 1980.
- Kupo, I., Yu. Mekler, and A. Eviatar, Detection of ionized sulphur in the Jovian magnetosphere, *Astrophys. Space Sci.*, 40, 63, 1976.
- Masursky, H., G. G. Schaber, L. A. Soderblom, and R. G. Strom, Preliminary geological mapping of Io, *Nature*, 280, 725, 1979.
- McNutt, R. L., and J. W. Belcher, Positive ion observations in the middle magnetosphere of Jupiter, *J. Geophys. Res.*, this issue.
- McNutt, R. L., J. W. Belcher, J. D. Sullivan, F. Bagenal, and H. S. Bridge, Departure from rigid corotation of plasma in Jupiter day-side magnetosphere, *Nature*, 280, 803, 1979.
- Mekler, Yu., and A. Eviatar, Time analysis of volcanic activity on Io by means of plasma observation, *J. Geophys. Res.*, 85, 1307-1310, 1980.
- Mekler, Yu., A. Eviatar, and I. Kupo, Jovian sulphur nebula, *J. Geophys. Res.*, 82, 2809, 1977.
- Michel, F. C., and P. A. Sturrock, Centrifugal instability of the Jovian magnetosphere and its interaction with the solar wind, *Planet. Space Sci.*, 22, 1501, 1974.
- Morgan, J. S., and C. B. Pilcher, Longitudinal variations of the Jovian [SII] emission, *Bull. Am. Astron. Soc.*, 10, 579, 1978.
- Nash, D. B., The Jupiter sulphur plasma ring (abstract), *Eos Trans. AGU*, 60, 307, 1979.
- Neugebauer, M., and A. Eviatar, An alternative interpretation of Jupiter's 'plasmopause,' *Geophys. Res. Lett.*, 3, 708, 1976.
- Pearl, J., R. Hanel, V. Kunde, W. Maguire, K. Fox, S. Gupta, C. Ponnampuruma, and F. Raulin, Identification of gaseous SO<sub>2</sub> and new upper limits on other gases on Io, *Nature*, 280, 755, 1979.
- Pilcher, C. B., Images of Jupiter's sulphur ring, *Science*, 207, 181, 1979.
- Pilcher, C. B., and J. S. Morgan, Detection of singly ionized oxygen around Jupiter, *Science*, 205, 297, 1979.
- Pilcher, C. B., and J. S. Morgan, The distribution of [SII] emission around Jupiter, *Astrophys. J.*, 238, 1980.
- Richardson, J. D., and G. L. Siscoe, Factors governing the ratio of inward to outward diffusing flux of satellite ions, *J. Geophys. Res.*, this issue.
- Richardson, J. D., G. L. Siscoe, F. Bagenal, and J. D. Sullivan, Time dependent plasma injection by Io, *Geophys. Res. Lett.*, 7, 37, 1980.
- Sandel, B. R., Longitudinal asymmetries in Jupiter's aurora and Io's plasma torus: Voyager observations, paper presented at the Conference on the Physics of the Jovian Magnetosphere, Rice Univ., Houston, Tex., Feb. 1980.
- Sandel, B. R., D. E. Shemansky, A. L. Broadfoot, J. L. Bertaux, J. E. Blamont, M. J. S. Belton, J. M. Ajello, J. B. Holberg, S. K. Atreya, T. M. Donahue, H. W. Moos, D. F. Strobel, J. C. McConnell, A. Dalgarno, R. Goody, M. B. McElroy, and P. Z. Takacs, Extreme ultraviolet observations from Voyager 2 encounters with Jupiter, *Science*, 206, 962, 1979.
- Scudder, J. D., E. C. Sittler, and H. S. Bridge, A survey of the plasma electron environment of Jupiter: A view from Voyager, *J. Geophys. Res.*, this issue.
- Shemansky, D. E., Mass loading and the diffusion loss rate of the Io plasma torus, *Astrophys. J.*, Dec. 1980.
- Siscoe, G. L., On the equatorial confinement and velocity space distribution of satellite ions in Jupiter's magnetosphere, *J. Geophys. Res.*, 82, 1641, 1977.
- Siscoe, G. L., Jovian plasmaspheres, *J. Geophys. Res.*, 83, 2118, 1978.
- Siscoe, G. L., and D. Summers, Centrifugally driven diffusion of Io-ionic plasma, *J. Geophys. Res.*, this issue.
- Smyth, W. H., and M. B. McElroy, Io's sodium cloud: Comparison of models and two-dimensional images, *Astrophys. J.*, 226, 336, 1978.
- Smyth, W. D., R. M. Nelson, and D. B. Nash, Spectral evidence for SO<sub>2</sub> frost of adsorbate on Io's surface, *Nature*, 280, 766, 1979.
- Strobel, D. F., UV observations of the Io plasma torus, paper presented at the Colloquium on the Satellites of Jupiter, Intl. Astron. Union, Kailua-Kona, Hawaii, May 1980.
- Sullivan, J. D., and F. Bagenal, In situ identification of various ionic species in Jupiter's magnetosphere, *Nature*, 280, 798, 1979.
- Trafton, L., The Jovian SII torus: Its longitudinal asymmetry, *Icarus*, 42, 111, 1980.
- Trauger, J. T., G. Munch, and F. L. Roesler, A study of the Jovian [SII] nebula at high spatial resolution, *Astrophys. J.*, 236, 1035, 1980.
- Vasyliunas, V. M., Deep space plasma measurements, in *Plasma Physics*, vol. 9B, *Methods of Experimental Physics*, edited by R. H. Lovbergs, p. 49, Academic, New York, 1971.
- Vogt, R. E., W. R. Cook, A. C. Cummings, T. L. Garrard, N. Gehrels, E. C. Stone, J. H. Trainor, A. W. Schardt, T. Conlon, N. Lal, and F. B. McDonald, Voyager 1: Energetic ions and electrons in the Jovian magnetosphere, *Science*, 204, 1003, 1979.
- Warwick, T. W., J. B. Pearce, A. C. Riddle, J. K. Alexander, M. D. Desch, M. L. Kaiser, J. R. Thieman, T. D. Carr, S. Gulkis, A. Boischoy, C. C. Harvey, and B. M. Pederson, Voyager 1 planetary radio astronomy observations near Jupiter, *Science*, 204, 955, 1979.

(Received July 28, 1980;  
revised November 3, 1980;  
accepted November 4, 1980.)